



# Physical meaning of the parameters used in fractal kinetic and generalised adsorption models of Brouers-Sotolongo

Taher Selmi, Mongi Seffen, Habib Sammouda, Sandrine Mathieu, Jacek Jagiello, Alain Celzard, Vanessa Fierro

## ► To cite this version:

Taher Selmi, Mongi Seffen, Habib Sammouda, Sandrine Mathieu, Jacek Jagiello, et al.. Physical meaning of the parameters used in fractal kinetic and generalised adsorption models of Brouers-Sotolongo. Adsorption - Journal of the International Adsorption Society, 2018, 24 (1), pp.11-27. 10.1007/s10450-017-9927-9 . hal-03563515

**HAL Id: hal-03563515**

**<https://hal.univ-lorraine.fr/hal-03563515>**

Submitted on 9 Feb 2022

**HAL** is a multi-disciplinary open access archive for the deposit and dissemination of scientific research documents, whether they are published or not. The documents may come from teaching and research institutions in France or abroad, or from public or private research centers.

L'archive ouverte pluridisciplinaire **HAL**, est destinée au dépôt et à la diffusion de documents scientifiques de niveau recherche, publiés ou non, émanant des établissements d'enseignement et de recherche français ou étrangers, des laboratoires publics ou privés.

# **Physical meaning of the parameters used in fractal kinetic and generalised adsorption models of Brouers-Sotolongo**

Taher Selmi<sup>1</sup>, Mongi Seffen<sup>1</sup>, Habib Sammouda<sup>1</sup>, Sandrine Mathieu<sup>2</sup>, Jacek Jagiello<sup>3</sup>, Alain Celzard<sup>4</sup> and Vanessa Fierro<sup>4\*</sup>

<sup>1</sup> Laboratory of Energy and Materials (LabEM). High School of Sciences and Technology of Hammam Sousse – Sousse University, BP 4011, Hammam Sousse, Tunisia.

<sup>2</sup> Institut Jean Lamour, UMR Université de Lorraine – CNRS 7198, Parc de Saurupt, CS 50840, 54011 Nancy Cedex, France.

<sup>3</sup> Micromeritics Instrument Corporation, 4356 Communications Drive, Norcross, GA 30093, USA.

<sup>4</sup> Institut Jean Lamour, UMR Université de Lorraine – CNRS 7198, BP 21042, 88051 Epinal Cedex 9, France.

\*Corresponding author (Vanessa Fierro)

Tel: + 33 372 74 96 77 Fax: + 33 372 74 96 38

E-mail address: [Vanessa.Fierro@univ-lorraine.fr](mailto:Vanessa.Fierro@univ-lorraine.fr)

## Abstract

The aim of the present study was to clarify the physical meaning of the parameters used in fractal kinetic and generalised isotherm models of Brouers-Sotolongo. For this purpose, adsorption of methylene blue (MB) and methyl orange (MO) onto four activated carbons (ACs) was carried out. These ACs were characterised in terms of composition, surface area, pore volumes and pore size distributions, carbon nanotexture and surface chemistry. Adsorption isotherms were carried out at 25°C, and at pH 2.5 and 8 for MO and MB, respectively, and fitted with Langmuir, Freundlich, Jovanovich, Hill-Sips (HS), Brouers-Sotolongo (BS), Brouers-Gaspard (BG) and General Brouers-Sotolongo (GBS) models. Adsorption kinetics were fitted by traditional pseudo-first and pseudo-second order models and compared to the Brouers-Sotolongo (BSf) fractal kinetic model. GBS and BSf were found to be the best models describing adsorption isotherms and kinetics, respectively. This finding suggests that MB and MO adsorption is probabilistic and closely correlated to the heterogeneous character of the adsorbent surface. Moreover, BSf and GBS parameters were correlated with surface area and amount of surface functional groups. In particular, higher surface area and amount of functional groups respectively decreased and increased the constants  $\tau_c$  and  $\alpha$  of the BSf stochastic model.

**Keywords:** Dyes adsorption; activated carbon; fractal kinetics; stochastic isotherm; surface heterogeneity; adsorption isotherms.

## 1. Introduction

Although water is an essential element to life on Earth, it is frequently contaminated by human activities, especially by those related to industries. Therefore, water depollution is an essential stage that should always be carried out by factories and chemical plants (Bello et al. 2013). One of the methods used for pollutant removal is adsorption on highly porous materials, among them activated carbons (ACs). ACs are characterized by their well-developed textural properties and are indeed commonly used for air treatment (Choi et al. 2016), biogas purification (Tian et al. 2009), gas storage (Sethia, Sayari 2016) and pollutants removal from water (Húmpola et al. 2016).

In order to understand the adsorption phenomena, different models can be applied for describing adsorption kinetics and isotherms data. For that purpose, stochastic isotherms and fractal kinetics have become increasingly employed (Sandro et al. 2009; Gaspard et al. 2006). Indeed, ACs can be considered as fractal materials due to their intricate porous network, developed during the activation process (Neimark 1992), and this has an influence on their adsorption properties. The adsorption process of a molecule dissolved in a solvent indeed takes place at the liquid-solid inter-phase with dimensional or topological constraints (Kopelman 1988). Thus, some physical properties of the adsorbate/adsorbent systems not only depend on the random behaviour of the mass distribution of adsorbent, but also on the fractal and stochastic character of its surface (Sokolowska et al. 2001).

Meilanov et al. (Meilanov et al. 2002) expressed the need of developing new studies of sorption kinetics based on fractals that would take the heterogeneity of adsorbents into account. This new approach was developed by Brouers and co-workers (Brouers, Sotolongo-Costa 2006; Brouers et al. 2005), who provided a new kinetic model called BSf including former models already applied to water treatment (Ben Hamissa et al. 2013) and to pharmacokinetics (Pereira 2010).

On the other hand, understanding adsorption isotherms, i.e., at equilibrium, remains a major way to predict the efficiency of some adsorbents for removing a given pollutant from water (Ncibi et al. 2008). Consequently, an abundant literature exists on the development of mathematical models and their suitability for describing adsorption phenomena. However, most of these models are empirical, are sometimes based on unrealistic assumptions and, finally, give little information on the physicochemical processes involved. For this reason, Brouers extended the empirical model of Langmuir in a more general one, called General Brouers-Sotolongo (GBS) model, based on a Burr distribution (Brouers 2014b).

Applying the aforementioned modern models presents many advantages compared to traditional ones. From the kinetics point of view, BSf allows determining valuable information with a very good accuracy such as adsorption capacity, fractal time exponent (see below for details), half-reaction time, and order of reaction. From the isotherms point of view, GBS allows determining the initial reaction kinetics at various concentrations of adsorbate, assessing the heterogeneity of ACs surface in terms of agglomeration and clustering of AC particles, or of fractal distribution of mesopores.

Herein, BSf and GBS models were used to describe adsorption kinetics and isotherms, respectively, of two dyes: methylene blue (MB) and methyl orange (MO), onto four ACs: F200, F300, Acticarbone® and Cecalite® (see below for description). These materials were also thoroughly characterised by elemental analysis, scanning electron microscopy (SEM), X-ray diffraction (XRD), Raman spectroscopy, thermogravimetry, mercury porosimetry, and adsorption-desorption of N<sub>2</sub> and CO<sub>2</sub> at -196°C and 0°C, respectively. Assessment of the surface functional groups of these ACs was obtained by a potentiometric titration technique. The initial pH,  $pH_{Initial}$ , and the pH of zero charge,  $pH_{PZC}$ , were also determined. We present correlations between the parameters of BSf and GBS models and the ACs' physicochemical

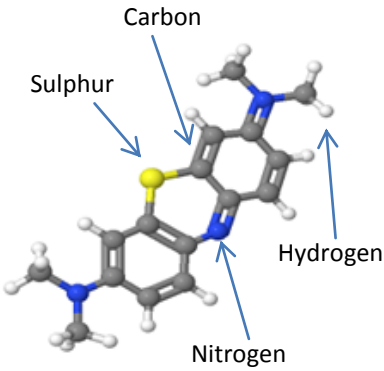
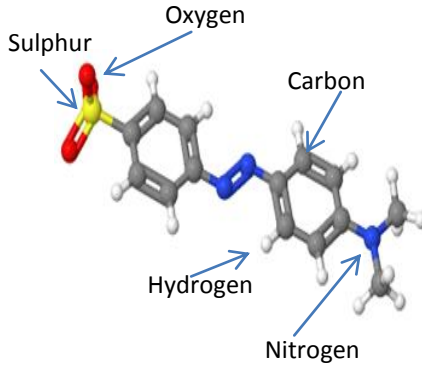
characteristics, namely porous texture and related parameters such as DFT surface area, and their chemical characteristics such as nature and amount of surface functional groups.

## 2. Materials and methods

### 2.1 Raw materials

Four commercial granular activated carbons (ACs) were used in this study. Filtrasorb 200 (F200) and Filtrasorb 300 (F300) from Calgon Corporation were obtained from a local textile industry (Chimitex, Tunisia). Acticarbone® and Cecalite® were purchased from CECA Company. All ACs were thoroughly washed with distilled water to remove surface impurities, followed by drying at 80°C for 48h.

**Table 1:** Main characteristics of dyes used in the present work.

Dye	MB (Cationic dye)	MO (Anionic dye)
Molecular structure	 $C_{16}H_{18}ClN_3S$	 $C_{14}H_{15}N_3O_3S$
Molecular weight ( $g \cdot mol^{-1}$ )	319.85	305.35
$\lambda$ (nm)	663	464

The basic dye, methylene blue (MB), and the acidic one, methyl orange (MO), both 85% pure, were purchased from Sigma-Aldrich. Stock solutions were prepared by dissolving accurately weighed amounts of MB and MO in distilled water to give a concentration of

1 g.L<sup>-1</sup>. The various solutions used in this study were then prepared by diluting the stock solution of either MB or MO with distilled water. **Table 1** shows the main characteristics of those dyes, such as their molecular structure and weight, their acidic or basic nature, and the optimum wavelength ( $\lambda$ ) used in UV-Vis experiments for their detection.

## 2.2 Activated carbon characterisation

The pore texture characterisation of ACs was carried out by adsorption-desorption studies of N<sub>2</sub> and CO<sub>2</sub> at -196°C and 0°C, respectively, in an ASAP 2020 manometric equipment (Micromeritics, USA). For each material, the BET model was applied to determine the apparent surface area,  $A_{BET}$  (m<sup>2</sup>.g<sup>-1</sup>), whereas the pore size distribution (PSD) was obtained by using two-dimensional (2D) version of the non-local density functional theory (NLDFT) with the Solution of Adsorption Integral Equation Using Splines (SAIEUS®) routine. SAIEUS® has the advantage of combining both CO<sub>2</sub> and N<sub>2</sub> adsorption data to get more accurate PSDs (Jagiello, Olivier 2013; Jagiello et al. 2015). The NLDFT method was also used to determine the surface area,  $S_{DFT}$  (m<sup>2</sup>.g<sup>-1</sup>), by integrating the PSD over the whole range of pore sizes (Centeno, Stoeckli 2010).

The total pore volume measurable by adsorption, or Gurvitch volume, was taken at the relative pressure of 0.97,  $V_{0.97}$  (cm<sup>3</sup>.g<sup>-1</sup>). The Dubinin-Raduskevich (DR) model (Dubinin 1981) was applied to obtain the microporous volume from the N<sub>2</sub> isotherm,  $V_{DR,N2}$  (cm<sup>3</sup>.g<sup>-1</sup>) on one hand, and from the CO<sub>2</sub> isotherm,  $V_{DR,CO2}$  (cm<sup>3</sup>.g<sup>-1</sup>) on the other hand. The average micropore volume,  $L_0$  (nm), was calculated from Stoeckli's equation (Stoeckli 1995):

$$L_0 = \frac{10.8}{E_0 - 11.4} \quad (1)$$

where  $E_0$  (kJ.mol<sup>-1</sup>) is the adsorption energy calculated by the DR model. The micropore volume was also calculated by application of the 2D-NLDFT model,  $V_{\mu,NLDFT}$  (cm<sup>3</sup>.g<sup>-1</sup>). The mesopore volume,  $V_{mes}$  (cm<sup>3</sup>.g<sup>-1</sup>), was obtained from the difference  $V_{0.97} - V_{\mu,NLDFT}$ .

Meso- and macropore size distributions were also determined by mercury porosimetry using an Autopore IV apparatus (Micromeritics, USA). Mercury intrusion was performed in two steps at low (0.001-0.24 MPa) and at high (0.24-414 MPa) pressure. Application of Washburn's equation (Washburn 1921), equation (2), allowed calculating the pore size as a function of the mercury pressure. Assuming cylindrical pores of diameter  $d$ , it reads:

$$d = - \frac{4 \sigma_{Hg} \cos \theta}{P} \quad (2)$$

where  $P$  is the pressure (MPa),  $\sigma_{Hg}$  is the surface tension of mercury (0.485 J.m<sup>-2</sup> at 20°C), and  $\theta$  is the contact angle (140°). Pores as narrow as 3.7 nm could be probed at the highest available pressure, 400 MPa.

XRD measurements were performed by using the Cu K $\alpha$  radiation generated by an X'Pert Pro diffractometer (Phillips, The Netherlands). The angle range used was 8°-100° with a scan step size of 0.0334°. Raman spectra were recorded in the range 0-3000 cm<sup>-1</sup> using a Labram HR800UV confocal Raman microscope (Horiba Jobin Yvon, Japan) equipped with a CCD detector cooled by Peltier effect. The morphology of the activated carbon was analysed by SEM with a FETQuanta 400 scanning electron microscope using an accelerating voltage of 3 kV.

Carbon, hydrogen, nitrogen and sulphur contents were determined with a Vario EL Cube elemental analyser (Elementar, Germany). Oxygen was also directly determined with the same equipment in a second step. Thermogravimetric analysis (TGA) was performed with an SDT Q600 V8.3 Build 101 thermal analyser (TA Instruments, USA) at a heating rate of 10°C.min<sup>-1</sup> in an air flow of 60 mL.min<sup>-1</sup>.

The pH at the point of zero charge, known as  $pH_{PZC}$ , is the pH at which the net charge of the surface is zero. The value of  $pH_{PZC}$  depends both on the nature and on the amount of functional groups at the surface. For determining it, 0.1 g of AC powder was put into contact with 20 mL of 0.1 mol.L<sup>-1</sup> NaCl solution and stirred for 48 h. Then, the suspension was



filtered and the equilibrium pH was measured. To determine the initial pH of ACs,  $pH_{Initial}$ , 0.1 g of AC powder was placed in 20 mL of distilled water (initial pH 5.7 due to dissolved atmospheric carbon dioxide) and equilibrated during the night. Then, the pH of the suspension was measured at room temperature.

Potentiometric titration was used to identify and to quantify the functional groups on the AC surface. For that purpose, 0.1 g of AC was placed in 50 mL of  $NaNO_3$  solution (0.01 mol.L<sup>-1</sup>), used both as electrolyte and as suspension medium, to which 1 mL of HCl (0.1 mol.L<sup>-1</sup>) was added. Then the solution was stirred overnight under N<sub>2</sub> saturation. The solution was then titrated with NaOH (0.1 mol.L<sup>-1</sup>) under N<sub>2</sub> saturation using a 905 Titrand automatic titrator (Metrohm, Switzerland) commanded with Tiamo<sup>®</sup> software V2.2. The  $pK_a$  distribution of the surface functional groups was calculated by determination of the proton binding function,  $f(pK_a)$ , and the total surface charge,  $Q$  (mmol.L<sup>-1</sup>), was obtained by applying the method of Jagiello (Jagiello 1994; Jagiello et al. 2000; Jagiello et al. 1995).

### 2.3 Adsorption of MB and MO

Adsorption studies were performed in batch experiments by adding 0.3 g of AC in 100 mL of MB and MO solutions at the desired concentration in the range 0.5 – 80 mg.L<sup>-1</sup>. The pH (2.5, 5 or 8) was adjusted by adding a small amount of either diluted HCl (0.1 mol.L<sup>-1</sup>) or diluted NaOH (0.1 mol.L<sup>-1</sup>) solution. The temperature (25, 35 or 50°C) was controlled with a thermostatic bath with an accuracy of  $\pm 1^\circ\text{C}$ . Suspensions of ACs in dye solutions were stirred with a magnetic device. Samples were investigated at different time intervals to measure dye removal and thus to perform kinetics studies. At each time increment, the residual dye concentration was determined by a Lambda 35 spectrophotometer (Perkin Elmer, USA) at a wavelength of 663 nm for MB and of 464 nm for MO (see again **Table 1**). The amount of adsorbed dye at equilibrium,  $q_e$  (mg.g<sup>-1</sup>), was calculated by application of equation (3):

$$q_e = \frac{(C_0 - C_e) V}{m} \quad (3)$$

where  $C_0$  and  $C_e$  (mg.L<sup>-1</sup>) are initial and equilibrium concentrations, respectively,  $V$  (L) is the volume of solution, and  $m$  (g) is the mass of AC in the suspension.

Thermodynamic parameters such as the variation of standard entropy,  $\Delta S^\circ$ , standard enthalpy,  $\Delta H^\circ$ , and standard free energy,  $\Delta G^\circ$ , were calculated as reported in Enaime et al. 2017.

193

### 2.3.1 Kinetic models

The pseudo-first order (PFO) kinetic model, also known as Lagergren's model, is generally used to describe solid / liquid adsorption processes. This model assumes that the rate of solute uptake is proportional to the difference between the saturation concentration and the amount of adsorbed solute as a function of time. PFO model can be described by equation (4):

$$q_t = q_{e,1} (1 - \exp(-k_1 t)) \quad (4)$$

where  $q_{e,1}$  is the amount of adsorbed dye at equilibrium (mg.g<sup>-1</sup>),  $k_1$  (min<sup>-1</sup>) is the rate constant of pseudo-first order adsorption, and  $t$  (min) is the time. The initial adsorption rate,  $h_1$  (mg.g<sup>-1</sup>.min<sup>-1</sup>) (Miao et al. 2016; Lagergren 1898) is calculated by equation (5):

$$h_1 = k_1 q_{e,1} \quad (5)$$

The pseudo-second-order model (PSO) kinetic model, also known as Ho and Mckay's model, is widely used for describing adsorption dynamics. In this model, the adsorption process, rather than the particle mass transfer process, is considered as the rate-limiting factor (Ho,McKay 1999). The PSO kinetic model can be written according to equation (6):

$$q_t = \frac{q_{e,2}^2 k_2 t}{1 + q_{e,2} k_2 t} \quad (6)$$

where  $q_{e,2}$  is the amount of adsorbed dye at equilibrium ( $\text{mg.g}^{-1}$ ) and  $k_2$  ( $\text{g.mg}^{-1}.\text{min}^{-1}$ ) is the rate constant of pseudo-second order adsorption.  $h_2$  ( $\text{mg.g}^{-1}.\text{min}^{-1}$ ) is the initial adsorption rate (Ho,McKay 1998, 1999) and is calculated as follows:

$$h_2 = k_2 q_{e,2}^2 \quad (7)$$

The equation of Brouers-Sotolongo (BS) takes into account the adsorption process complexity (Brouers et al. 2004; Brouers 2014a), and has been recently used in various works (Brouers,Sotolongo-Costa 2006; Gaspard et al. 2006; Ben Hamissa et al. 2013; Kesraoui et al. 2016). The BS equation reads:

$$q_{n,\alpha}(t) = q_e \left[ 1 - \left( 1 + (n-1) \left( \frac{t}{\tau_{n,\alpha}} \right)^\alpha \right)^{\frac{-1}{(n-1)}} \right] \quad (8)$$

If we use the deformed  $n$ -exponential (Brouers,Sotolongo-Costa 2006)

$$\text{Exp}_n(x) = [1 - (n-1)x]^{\frac{-1}{(n-1)}}, \quad (9)$$

the BSf model can therefore be written as shown in equation (10):

$$q(t) = q_e \left[ 1 - \text{Exp}_n \left( - \left( \frac{t}{\tau_{n,\alpha}} \right)^\alpha \right) \right] \quad (10)$$

where  $\alpha$  is the fractal time exponent,  $n$  is a fractional (non-integer) reaction order, and  $q_{n,\alpha}(t)$  and  $q_{e,BS}$  are the adsorbed amounts at time  $t$  and at saturation, respectively.  $\tau_c$  is the characteristic time of the complex kinetics, which depends on the initial concentration and on the two exponents  $n$  and  $\alpha$ . When  $\alpha = 1$  and  $n = 1$ , the PFO equation is obtained, whereas  $\alpha = 1$  and  $n = 2$  leads to PSO. If  $\alpha \neq 1$  and  $n = 1$ , the Weibull distribution is obtained and reads:

$$q_{1,\alpha}(t) = q_{e,W} \left[ 1 - \text{Exp} \left( - \left( \frac{t}{\tau_c} \right)^\alpha \right) \right]. \quad (11)$$

For  $\alpha \neq 1$  and  $n = 2$ , the Hill equation is obtained and reads:

$$q_{2,\alpha}(t) = q_{e,H} \left[ 1 - \left( 1 + \left( \frac{t}{\tau_c} \right)^\alpha \right)^{-1} \right]. \quad (12)$$

The “half reaction” time  $\tau_{1/2}$ , given by equation (14), is the necessary time to adsorb half of the initial concentration, and it can be derived from equation (13) using the deformed logarithm (Brouers 2014a):

$$\left[1 + (n-1) \left(\frac{t}{\tau_c}\right)^\alpha\right]^{\frac{-1}{(n-1)}} = \frac{1}{2} \quad (13)$$

$$\tau_{1/2} = \tau_c \left(\frac{2^{(n-1)} - 1}{n-1}\right)^{1/\alpha}. \quad (14)$$

### 2.3.2 Adsorption isotherm models

In the present paper, six models were used to study the adsorption isotherms: Langmuir (Langmuir 1918), Freundlich (Freundlich 1906), Brouers-Sotolongo (BS) (Brouers 2014b), Jovanovich (Jovanović 1969), Hill-Sips (HS) (Sips 1948) and General Brouers-Sotolongo (GBS) (Brouers et al. 2005; Brouers 2014b). The first five models can be obtained by giving well-defined values to the parameters  $a$  and  $c$  in the GBS equation:

$$q_{e\text{ GBS}} = q_{e\text{ max}} \left(1 - \text{Exp}_c \left[-\left(\frac{C_e}{b}\right)^a\right]\right) = q_{e\text{ max}} \left(1 - \left[1 + c \left(\frac{C_e}{b}\right)^a\right]^{-1/c}\right) \quad (15)$$

Thus, for  $c = 1$  and  $a = 1$ , the Langmuir isotherm is recovered:

$$q_{eL} = q_{e\text{ max}L} \left(1 - \left[1 + \left(\frac{C_e}{b}\right)\right]^{-1}\right) = q_{e\text{ max}L} \frac{C_e}{b + C_e}. \quad (16)$$

For  $c = 0$ , we get the normal Brouers-Sotolongo (BS) isotherm:

$$q_{e\text{ BS}} = q_{e\text{ maxBS}} \left(1 - \text{Exp} \left[-\left(\frac{C_e}{b}\right)^a\right]\right), \quad (17)$$

and at low concentration,  $C_e \ll b$ , one gets the Freundlich isotherm:

$$q_{eF} = K_F C_e^a \quad (18)$$

For  $c = 0$  and  $a = 1$ , we find the Jovanovich isotherm:

$$q_{eJ} = q_{e\text{ max}J} \left(1 - \text{Exp} \left[-\left(\frac{C_e}{b}\right)\right]\right), \quad (19)$$

And finally, for  $c = 1$ , we get the HS isotherm:

$$q_{eHS} = q_{e\max HS} \left( 1 - \left[ 1 + \left( \frac{C_e}{b} \right)^a \right]^{-1} \right). \quad (20)$$

It was shown that the constant  $c$  should range between 0 and 1 (Brouers, Al-Musawi 2015). However, if the isotherm does not reach saturation, the constant  $c$  can be higher than 1 and therefore the results have no physical meaning in a statistical approach. As it is difficult to choose between HS and BS isotherm (i.e., between  $c = 0$  and 1), Brouers proposed to fit the adsorption isotherms with  $c = 0.5$  (Brouers, Al-Musawi 2015), leading to what is known as the Brouers-Gaspard (BG) isotherm, which reads:

$$q_{eGBS} = q_{e\max} \left( 1 - \text{Exp}_{c=0.5} \left[ - \left( \frac{C_e}{b} \right)^a \right] \right) = q_{e\max} \left( 1 - \left[ 1 + \frac{1}{2} \left( \frac{C_e}{b} \right)^a \right]^{-2} \right). \quad (21)$$

The knowledge of constants  $a$ ,  $b$  and  $c$  allows determining  $C_e$  or a given percentage of  $C_e$ ; in particular,  $Ce_{\frac{1}{2}}$  (50% of  $C_e$ ) was calculated with the following equations.

In the GBS case, we have:

$$Ce_{\frac{1}{2}} = b \left( \frac{2^c - 1}{c} \right)^{\frac{1}{a}}, \quad (22)$$

in BS case:

$$Ce_{\frac{1}{2}} = b (\ln 2)^{\frac{1}{a}}, \quad (23)$$

in Jovanovich case:

$$Ce_{\frac{1}{2}} = b \ln 2, \quad (24)$$

in HS and Langmuir case:

$$Ce_{\frac{1}{2}} = b, \quad (25)$$

and finally in BG case:

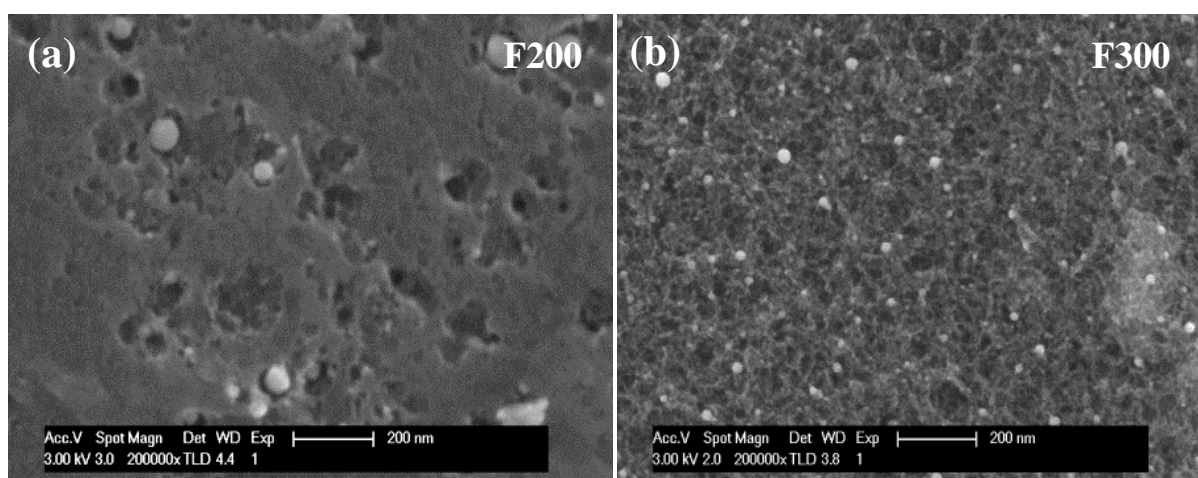
$$Ce_{\frac{1}{2}} = b (2\sqrt{2} - 2)^{\frac{1}{a}}. \quad (26)$$

### 3. Results and discussion

#### 3.1 Physicochemical characteristics of ACs

Physicochemical properties of all ACs in terms of elemental analysis, thermal stability in air flow, carbon nanotexture and crystalline structure are given in Supplementary Information. **Table SI 1** thus presents the C, H, O and N contents of all materials, whereas results of thermogravimetric, Raman and X-ray diffraction studies are given in **Fig. SI 1**, **Fig. SI 2**, and **Fig. SI 3**, respectively. The corresponding discussion is also provided in the Supplementary Information.

**Fig 1** shows the morphology of these ACs as seen by SEM. These images, obtained by using secondary electrons, demonstrate some important differences between materials in terms of grain morphology, surface roughness and open porosity. F200 (**Fig 1a**) has a heterogeneous surface with large pores of broad distribution of sizes. Regarding F300 (**Fig 1b**), the pores are much smaller and the surface appears to be very rough. Acticarbone® (**Fig 1c**) has a completely different morphology based on microspheres, somewhat similar to what is obtained by hydrothermal treatment of biomass (Braghiroli et al. 2015). Finally, Cecalite® (**Fig 1d**) presents a rather smooth surface with well-dispersed mesopores of rather equal sizes.



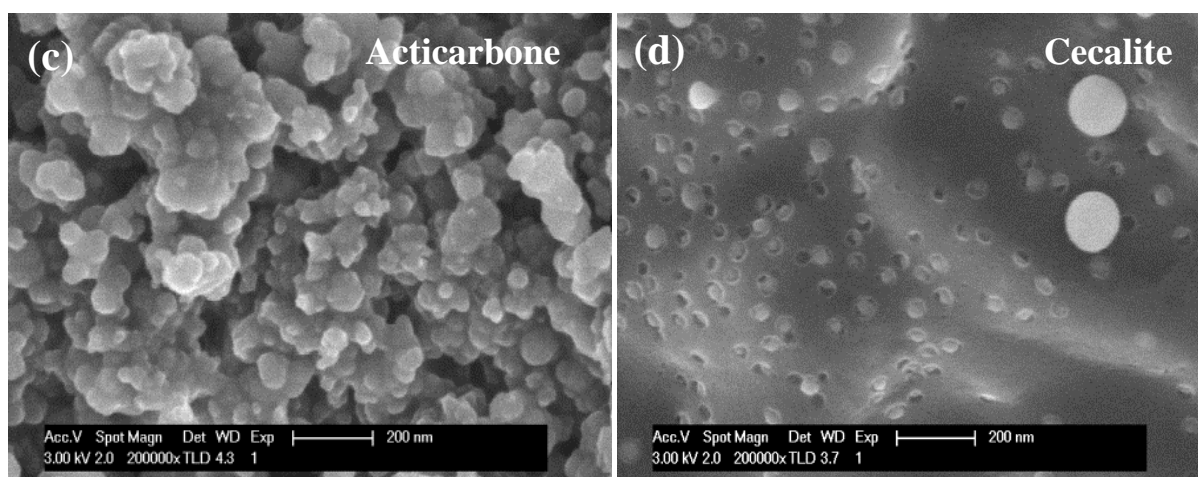


**Fig 1** SEM pictures of activated carbons used here: (a) F200, (b) F300, (c) Acticarbone®, and (d) Cecalite®.

The adsorption-desorption isotherms of  $N_2$  and  $CO_2$  for the four activated carbons are shown in **Fig 2a** and **Fig 2b**, respectively. **Fig 2c** shows the corresponding PSDs obtained by application of the 2D-NLDFT method to both  $N_2$  and  $CO_2$  isotherms (Jagiello, Olivier 2013).  $N_2$  adsorption isotherm at  $-196^\circ C$  on Cecalite® was type Ia, characteristic of a microporous material with adsorption occurring by primary filling of microspores at very low relative pressure  $P/P_0$  (IUPAC 2015). The adsorption isotherms of F200 and F300 were type Ib, characteristic of microporous materials with micropores wider than those of type Ia present in Cecalite®. Cooperative filling as well as primary filling indeed takes place on a wider  $P/P_0$  range than for type Ia (IUPAC 2015). No horizontal plateau was clearly achieved, indicating pore widening; these isotherms also showed a type H4 hysteresis loop, characteristic of slit-shaped pores according to the IUPAC classification (IUPAC 2015). Finally, the  $N_2$  isotherm on Acticarbone® was type IIb, with high adsorption at low  $P/P_0$ , and a well-developed hysteresis loop, type H4, showing the simultaneous presence of micro and mesopores. The hysteresis loop of Acticarbone® was more pronounced than that of F300, which means that its mesoporous volume was more developed.

**Table 2:** Textural characteristics of the four activated carbons obtained by adsorption-desorption of N<sub>2</sub> at -196°C and of CO<sub>2</sub> at 0°C, applying BET, DR and 2D-NLDFT methods.

Materials	$A_{BET}$ (m <sup>2</sup> .g <sup>-1</sup> )	$S_{DFT}$ (m <sup>2</sup> .g <sup>-1</sup> )	$V_{DR, N_2}$ (cm <sup>3</sup> .g <sup>-1</sup> )	$V_{DR, CO_2}$ (cm <sup>3</sup> .g <sup>-1</sup> )	$V_{0.97}$ (cm <sup>3</sup> .g <sup>-1</sup> )	$V_{\mu, NLDFT}$ (cm <sup>3</sup> .g <sup>-1</sup> )	$V_{mes}$ (cm <sup>3</sup> .g <sup>-1</sup> )	$V_{mes}$ (%)
F200	795	971	0.28	0.24	0.39	0.30	0.09	22
F300	884	1003	0.35	0.28	0.43	0.34	0.09	21
Acticarbhone®	1014	967	0.35	0.18	0.56	0.38	0.16	29
Cecalite®	582	830	0.22	0.23	0.24	0.24	0.01	3

**Fig 2d** shows the PSDs obtained by mercury porosimetry. The highest porosity, i.e., the volume fraction of macropores and of mesopores available to mercury, corresponds to Acticarbhone®, around 54.3 %. The porosity measurable with this technique for the other ACs was 39.7%, 35.3% and 38.0% for F200, F300 and Cecalite®, respectively. The mercury intrusion-extrusion curves are given in **Fig SI 4** of the supplementary information, evidencing the entrapment of mercury when the pressure was decreased. This finding suggests the presence of a significant amount of ink bottle-shaped pores, but also that irreversible compression may have occurred under pressure. More information is also given in **Table SI 2**, suggesting that all ACs are different either in terms of macro/mesopore size (e.g. when F200 and Cecalite® are compared) or in terms of amounts of pores of similar sizes (e.g. when F300 and Acticarbhone® are compared).

reports the textural characteristics obtained from N<sub>2</sub> and CO<sub>2</sub> isotherms. The values of  $A_{BET}$  ranged from 582 m<sup>2</sup>.g<sup>-1</sup> for Cecalite® to 1014 m<sup>2</sup>.g<sup>-1</sup> for Acticarbhone®.  $S_{DFT}$  values were higher than those of  $A_{BET}$  for F200, F300 and Cecalite®, meaning that these ACs have an important fraction of narrow microporosity in which only one single nitrogen monolayer can be adsorbed. On the contrary,  $A_{BET}$  of Acticarbhone® was higher than  $S_{DFT}$ . This means that the pore texture is highly developed with wider micropores, wherein a supplementary nitrogen



molecule can be accommodated between two layers of  $N_2$  adsorbed onto the pore walls. The volume of Dubinin-Raduskevich accessible to  $N_2$ ,  $V_{DR,N_2}$ , was always higher than  $V_{DR,CO_2}$  except for Cecalite®; this means that there is also an important fraction of micropores wider than 1 nm because  $CO_2$  can probe pores narrower than 1 nm. In agreement with such finding, the average micropore diameter,  $L_0$ , calculated by application of the DR model to the  $N_2$  isotherms, was indeed 0.7, 0.8, 1.1 and 0.6 nm for F200, F300, Acticarbone® and Cecalite®, respectively. Acticarbone® had the highest fraction of mesoporosity (29 % of total volume measurable by gas adsorption) while Cecalite® only had 3%. F200 and F300 had intermediate and nearly identical mesoporous fractions of 22 and 21 %, respectively. The higher supermicroporosity and mesoporosity of Acticarbone® is in good agreement with its higher value of  $A_{BET}$  with respect to  $S_{DFT}$ .

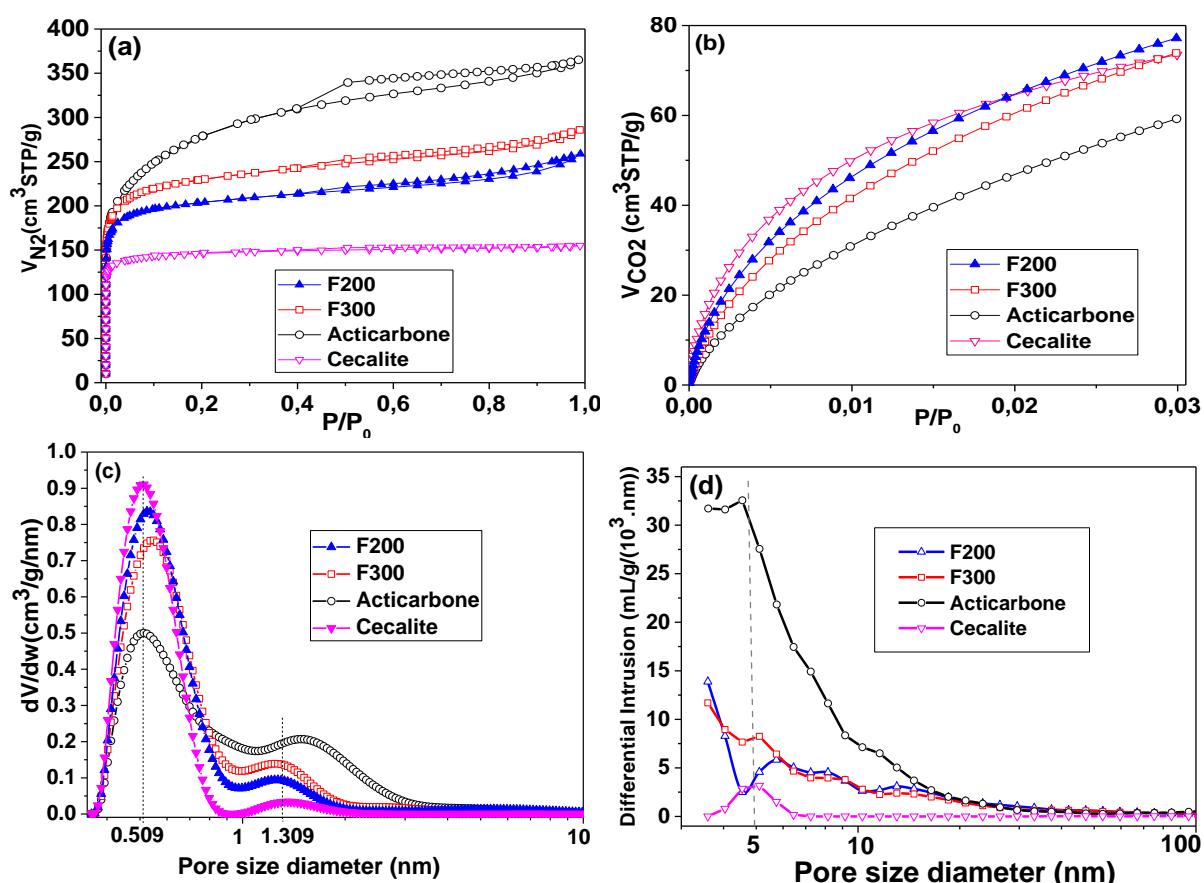


**Fig 2** Adsorption-desorption isotherms of: (a)  $N_2$  at  $-196^\circ\text{C}$ , (b)  $CO_2$  at  $0^\circ\text{C}$ , and (c) PSDs obtained from  $N_2$  and  $CO_2$  adsorption data; (d) PSDs obtained by mercury intrusion.

347

348 **Table 2:** Textural characteristics of the four activated carbons obtained by adsorption-  
 349 desorption of N<sub>2</sub> at -196°C and of CO<sub>2</sub> at 0°C, applying BET, DR and 2D-NLDFT methods.

Materials	$A_{BET}$ (m <sup>2</sup> .g <sup>-1</sup> )	$S_{DFT}$ (m <sup>2</sup> .g <sup>-1</sup> )	$V_{DR, N_2}$ (cm <sup>3</sup> .g <sup>-1</sup> )	$V_{DR, CO_2}$ (cm <sup>3</sup> .g <sup>-1</sup> )	$V_{0.97}$ (cm <sup>3</sup> .g <sup>-1</sup> )	$V_{\mu, NLDFT}$ (cm <sup>3</sup> .g <sup>-1</sup> )	$V_{mes}$ (cm <sup>3</sup> .g <sup>-1</sup> )	$V_{mes}$ (%)
F200	795	971	0.28	0.24	0.39	0.30	0.09	22
F300	884	1003	0.35	0.28	0.43	0.34	0.09	21
Acticarbhone®	1014	967	0.35	0.18	0.56	0.38	0.16	29
Cecalite®	582	830	0.22	0.23	0.24	0.24	0.01	3

350

351 **Fig 2d** shows the PSDs obtained by mercury porosimetry. The highest porosity, i.e., the  
 352 volume fraction of macropores and of mesopores available to mercury, corresponds to  
 353 Acticarbhone®, around 54.3 %. The porosity measurable with this technique for the other ACs  
 354 was 39.7%, 35.3% and 38.0% for F200, F300 and Cecalite®, respectively. The mercury  
 355 intrusion-extrusion curves are given in **Fig SI 4** of the supplementary information, evidencing  
 356 the entrapment of mercury when the pressure was decreased. This finding suggests the  
 357 presence of a significant amount of ink bottle-shaped pores, but also that irreversible  
 358 compression may have occurred under pressure. More information is also given in **Table SI**  
 359 **2**, suggesting that all ACs are different either in terms of macro/mesopore size (e.g. when  
 360 F200 and Cecalite® are compared) or in terms of amounts of pores of similar sizes (e.g. when  
 361 F300 and Acticarbhone® are compared).

362

363 **Fig 3** shows the acidity distribution functions,  $f(pK_a)$ , of the four ACs. The resolution of  
 364 this method was demonstrated by using solutions of organic acids with known  $pK_a$  values  
 365 (Jagiello et al. 2000; Jagiello et al. 1995). At least four important functional groups were  
 366 evidenced, except for F300, which presented only two. Traditionally,  $pK_a = 3-8$  is the region

of carboxylic acids while  $pK_a = 8-10$  corresponds to the phenolic region (Bandosz et al. 1993; Benaddi et al. 2000). The  $pK_a$  distribution curves showed the predominance of strongly basic species such as hydroxyl functionalities (Zhang et al. 2015; Seredych et al. 2016). The amount of very basic groups,  $pK_a > 10$ , accounts for nearly half of all functional groups of all ACs. Therefore, all materials produced a pH slightly higher (1 to 1.4 pH unit) than that of the water in which they were suspended, as shown by the values of  $pH_{Initial}$  presented in **Table SI 3**. F200 and Acticarbone® had similar total amounts of surface groups, 1.145 and 1.150 mmol.g<sup>-1</sup>, respectively, and also a very similar  $pH_{PZC}$ , 7.20 and 7.36, respectively. F300 and Cecalite® showed much less functional groups, 0.605 and 0.787 mmol.g<sup>-1</sup>, respectively, and slightly higher  $pH_{PZC}$  of 8.03 and 7.75, respectively. **Table SI 3** also shows the results of the potentiometric titration as well as  $pH_{PZC}$  and  $pH_{Initial}$  values for all ACs studied.

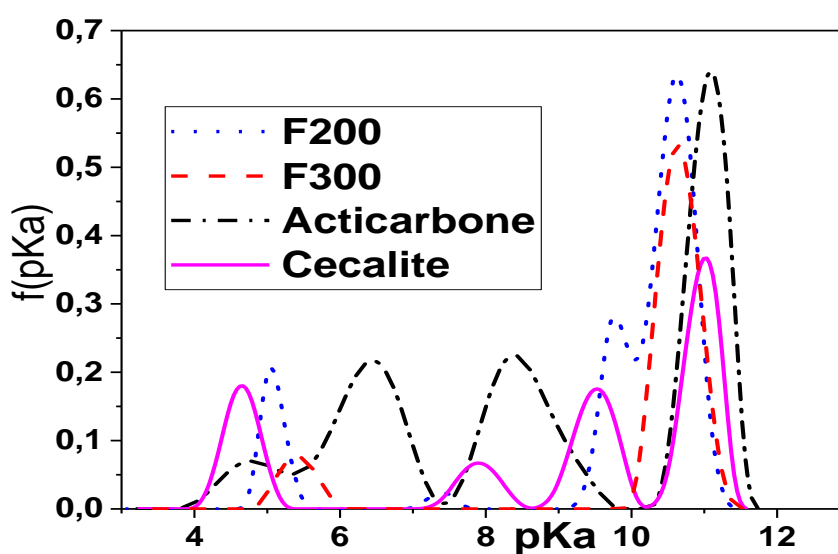


**Fig 3** Density of functional groups of all studied ACs.

### 3.2 Adsorption of dyes

In order to explain the adsorption kinetics and isotherms of MB and MO, the experimental data were non-linearly fitted by using the *Levenberg Marquardt* iteration algorithm supplied with OriginPro 2016 Software®. PFO, PSO and BSf models were used to fit the kinetic data.

Langmuir, Freundlich, Jovanovich, HS, BS, BG and GBS models were used to fit the adsorption isotherms.

### 3.2.1 Effect of pH, temperature and thermodynamic analysis on MB and MO adsorption

**Fig 4** shows the effect of pH and temperature on the removal of MB and MO by ACs. The removal efficiency was enhanced when the temperature increased from 25 to 50°C, indicating the endothermic character of the adsorption (Kesraoui et al. 2016). The removal efficiency also increased when the pH increased from 2.5 to 8 for MB adsorption, but decreased for MO adsorption. Rodríguez et al. found a similar result for the adsorption of MB and Orange II dyes on ACs (Rodríguez et al. 2009). This finding may be ascribed to the increase or decrease of repulsive and attractive forces between surface functional groups of ACs and anion of dyes used, which depend on  $pH_{PZC}$  values. The anionic dyes are indeed favourably adsorbed at acidic  $pH < pH_{PZC}$ , at which the surface is positively charged. On the contrary, cationic dyes are better adsorbed on anionic sites of the adsorbent surface when the latter is globally negatively charged for  $pH > pH_{PZC}$  (Kesraoui et al. 2016).

Thermodynamic parameters such as Gibbs free energy  $\Delta G^\circ$  (kJ.mol<sup>-1</sup>), enthalpy  $\Delta H^\circ$  (kJ.mol<sup>-1</sup>), and entropy  $\Delta S^\circ$  (J.mol<sup>-1</sup>.K<sup>-1</sup>) were determined and are listed in

**Table 3.** The positive value of  $\Delta H^\circ$  for MB and MO in the presence of all ACs indicates the endothermic nature of the adsorption process. The positive values of  $\Delta S^\circ$  correspond to an increase of disorder at the interface between dyes and the surface of all samples used (Bouhamed et al. 2016; Kesraoui et al. 2016), the absolute values reflecting the affinity of the adsorbents for those dyes. With only one exception, MO on Cecalite® at 25°C, the values of  $\Delta G^\circ$  were always negative, showing the spontaneous nature of adsorption of MB and MO onto all ACs used (Acosta et al. 2016).  $\Delta G^\circ$  indeed varied from -10.70 to -19.51 kJ.mol<sup>-1</sup>,

suggesting the highly favourable adsorption of those molecules onto Acticarbone®, F300, and F200. In contrast, adsorption was only slightly favourable on Cecalite®, which exhibited absolute values of  $\Delta G^\circ$  one order of magnitude lower than those observed for the other ACs. And especially, MO adsorption at pH 2.5 was even unfavourable at room temperature, as shown by the positive value of  $\Delta G^\circ$  and the correspondingly lower values of  $\Delta H^\circ$  and  $\Delta S^\circ$  with respect to those of other activated carbons. A similar result was reported elsewhere (Rodríguez et al. 2009).

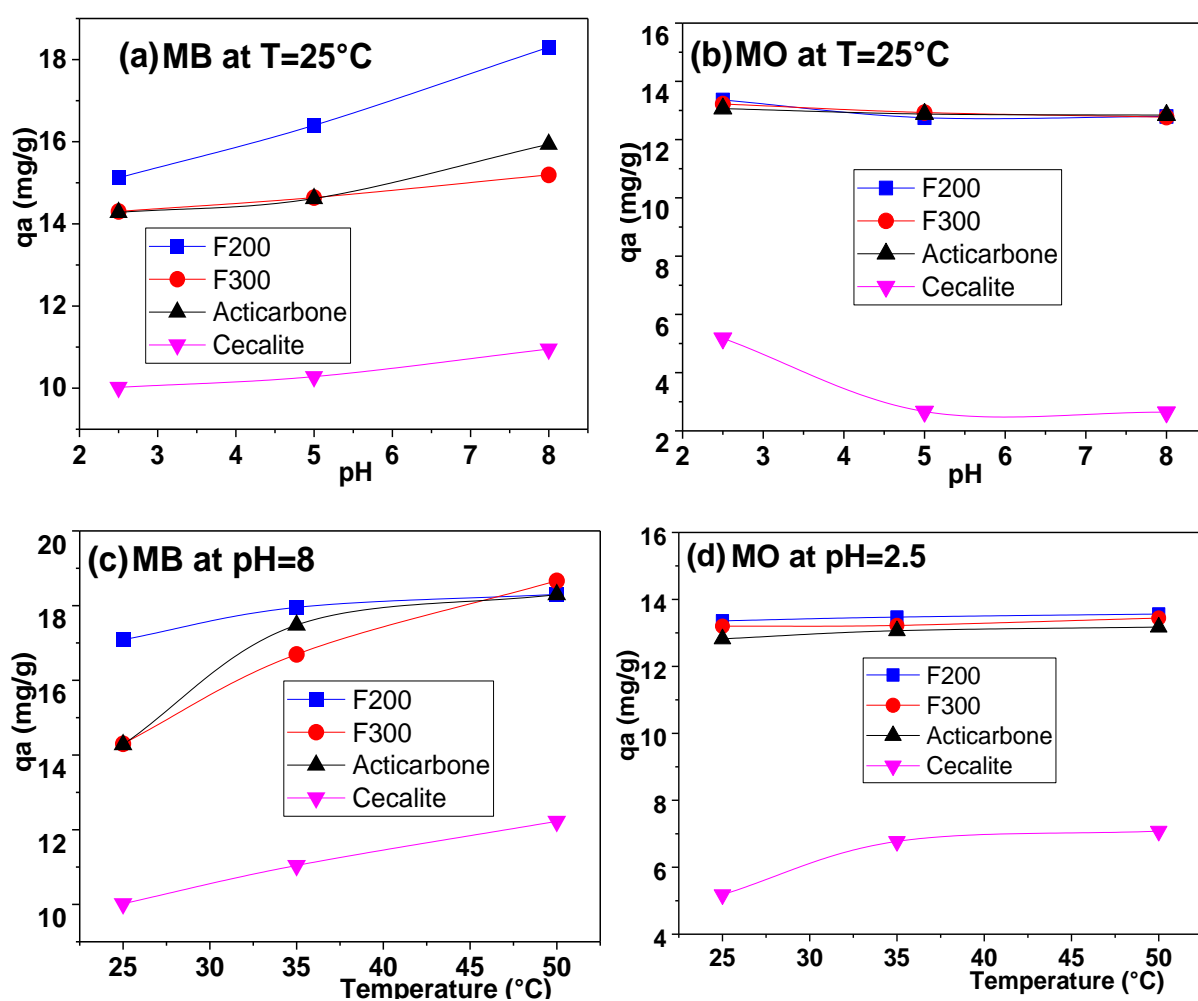


**Fig 4** Effect of: (a, b) pH at 25°C and (c, d) temperature, on the adsorbed amount at equilibrium of: (a, c) MB at pH 8, and (b, d) MO at pH 2.5, onto all ACs ( $C_0 = 40 \text{ mg.L}^{-1}$ )

**Table 3:** Thermodynamic parameters for the adsorption of MB and MO onto all activated carbons samples at different temperatures and  $C_0 = 40 \text{ mg.L}^{-1}$ .

Samples	Dye	pH	$\Delta H^\circ$ (kJ.mol <sup>-1</sup> )	$\Delta S^\circ$ (J.mol <sup>-1</sup> .K <sup>-1</sup> )	$\Delta G^\circ$ (kJ.mol <sup>-1</sup> )		
					25°C	35°C	50°C
F200	MB	8	49.40	212.50	-14.30	-15.60	-19.50
	MO	2.5	16.10	95.70	-12.50	-13.30	-14.90
F300	MB	8	16.60	100.70	-13.40	-14.30	-15.90
	MO	2.5	63.20	247.60	-10.70	-12.90	-16.80
Acticarbhone®	MB	8	20.10	112.80	-13.20	-15.10	-16.00
	MO	2.5	25.40	121.80	-11.20	-11.70	-14.20
Cecalite®	MB	8	11.10	40.80	-1.20	-1.30	-2.20
	MO	2.5	19.00	61.30	1.00	-0.20	-0.60

### 3.2.2 Kinetic models

**Table 4** shows the kinetic parameters obtained for initial dye concentrations equal to 10, 40, 60, and 80 mg.L<sup>-1</sup> by application of the BSf model to the MB and MO adsorption data on Acticarbhone®. Equivalent data for the other 3 ACs are given in **Table SI 4**, **Table SI 5** and **Table SI 6** of the Supplementary Information. Fits were performed for values of  $n = 1$ , 1.5 and 2. Although the determination parameter,  $R^2$ , was always very high, the best fit for MB adsorption was achieved with the reaction order fixed at  $n = 1$ . Similar results were obtained when MB was biosorbed on *Agave Americana* fibres (Ben Hamissa et al. 2013), and when Indigo Carmine dye was adsorbed on activated carbon (Kesraoui et al. 2016). Based on the determination coefficient, and given the fact that  $\alpha$  describes better the heterogeneity of the surface when its value doesn't exceed 1 (Brouers 2014a), the kinetics is also expected to be of order 1. For MO, excellent fits were also obtained with  $n = 1$  although the highest values of  $R^2$  were obtained with  $n = 1.5$  or  $n = 2$  (see the data for the other ACs in **Table SI 4**, **Table SI 5** and **Table SI 6** of the Supplementary Information).

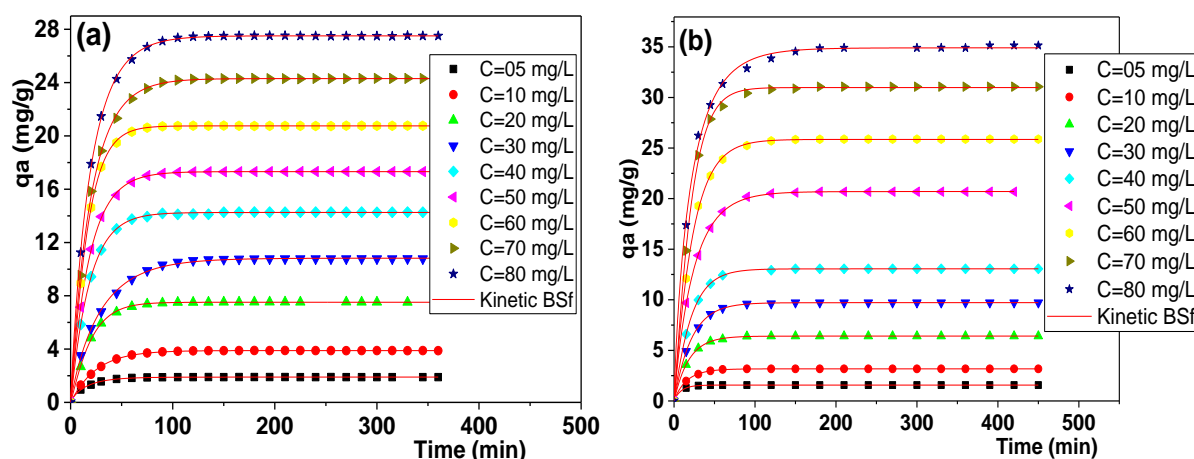
Since, on average, excellent fits were found for all ACs with  $n = 1$ , which is the value leading most frequently to the highest determination coefficient, it was assumed that the

adsorption of MB and MO dyes on all ACs follows first-order kinetics. Fixing the reaction order  $n = 1$  was indeed necessary to compare the BSf kinetics to other models.

**Fig 5** shows the experimental kinetic data and the calculated curves when  $n$  was fixed to 1 for MB and MO adsorption on Acticarbhone®: a very good fit was obtained for all initial concentrations from 5 to 80 mg.L<sup>-1</sup>, for both dyes. Equally good fits were obtained for the other three ACs, and the corresponding results are given in **Fig SI 5**.

**Table 4:** Effect of reaction order  $n$  on BSf kinetics parameters obtained by non-linear fit of the adsorption of MB at pH 8 and MO at pH 2.5 on Acticarbhone® at 25°C.

		Initial concentration of MB and MO (mg.L <sup>-1</sup> )											
		10			40			60			80		
		$\tau_c$	$\alpha$	$R^2$	$\tau_c$	$\alpha$	$R^2$	$\tau_c$	$\alpha$	$R^2$	$\tau_c$	$\alpha$	$R^2$
MB	$n = 1$	25.14	1.01	<u>1.00</u>	18.61	1.02	<u>1.00</u>	16.79	1.09	<u>1.00</u>	19.42	0.93	<u>1.00</u>
	$n = 1.5$	20.09	1.32	0.998	14.98	1.36	0.999	13.69	1.47	1.00	15.45	1.26	0.999
	$n = 2$	17.29	1.62	0.996	13.00	1.72	0.998	12.01	1.89	0.998	13.31	1.60	0.998
MO	$n = 1$	15.70	0.95	<u>1.00</u>	22.52	1.11	0.999	23.00	1.03	1.00	22.09	0.84	0.998
	$n = 1.5$	13.07	1.39	0.999	17.16	1.41	<u>1.00</u>	18.72	1.40	<u>1.00</u>	17.59	1.16	0.999
	$n = 2$	11.86	1.91	1.00	15.15	1.84	0.999	16.46	1.81	0.999	15.30	1.5	<u>1.00</u>



455 **Fig 5** BSf (1, $\alpha$ ) kinetics model applied to the adsorption of: (a) MB at pH 8 and (b) MO at pH  
 456 2.5, onto Acticarbone® for different initial concentrations at 25°C.

458 **Fig SI 6** shows the non-linear fit of the adsorption data kinetics of MB at pH 8 and of MO  
 459 at pH 2.5 onto Acticarbone® by the models listed in the experimental section (i.e., Pseudo-  
 460 first-order (PFO), Pseudo-second-order (PSO) and Brouers-Sotolongo fractal (BSf(1, $\alpha$ ))). The  
 461 corresponding kinetic models parameters are summarised in **Table 5**. For selecting the best  
 462 one, values of determination coefficients,  $R^2$ , and errors,  $\chi^2$ , were examined. For example, for  
 463 MO adsorption on F300 samples,  $R^2$  was found to be equal to 0.998, 0.992 and 1 for PFO,  
 464 PSO and BSf(1, $\alpha$ ), respectively, hence the Weibull equation ( $\alpha \neq 1$  and  $n = 1$ ) was the most  
 465 relevant one for fitting the kinetic data.

467 **Table 5:** Kinetic parameters obtained by fitting the experimental data with PFO, PSO and BSf  
 468 models ( $C_0=40$  mg.L<sup>-1</sup> of MO at pH 2.5 and of MB at pH 8, at 25°C).

	MB				MO			
Samples	F200	F300	Acticarbone	Cecalite	F200	F300	Acticarbone	Cecalite
$q_{e,exp}$	18.30	14.30	14.28	10.02	13.36	13.22	13.06	5.18
PFO								
$q_{e,1}$	18.37	14.26	14.26	11.11	13.25	13.15	13.07	4.72
$k_1$	0.02	0.04	0.05	0.007	0.02	0.06	0.05	0.01
$R^2$	0.992	<u>0.999</u>	1	0.988	0.996	0.998	1	0.954
$\chi^2$	0.224	<u>0.009</u>	0.002	0.138	0.055	0.019	0.002	0.101
$h_1$	0.36	0.64	0.77	0.07	0.31	0.73	0.63	0.05
PSO								
$q_{e,2}$	21.35	15.31	15.13	15.27	14.73	13.74	13.74	5.70
$k_2$	0.001	0.005	0.006	0.001	0.002	0.008	0.006	0.002
$R^2$	0.974	0.979	0.976	0.999	0.995	0.992	0.981	0.982
$\chi^2$	0.728	0.243	0.253	0.114	0.082	0.091	0.220	0.038
$h_2$	0.50	1.10	1.40	0.09	0.47	1.45	1.17	0.07
BSf(1, $\alpha$ )								
$q_{e,BS}$	18.23	14.26	14.25	14.10	13.41	13.19	13.06	8.03



$\tau_c$	49.94	22.19	18.61	251.47	44.03	17.33	21.02	453.11
$\tau_{1/2}$	16.73	6.60	5.71	53.73	10.54	4.24	6.61	43.03
$\alpha$	1.10	0.99	1.02	0.78	0.84	0.85	1.04	0.51
$R^2$	<u>0.993</u>	0.999	<u>1</u>	<u>0.993</u>	<u>1</u>	<u>1</u>	<u>1</u>	<u>0.997</u>
$\chi^2$	<u>0.199</u>	0.010	<u>0.002</u>	<u>0.083</u>	<u>0.004</u>	<u>0.004</u>	<u>0.001</u>	<u>0.007</u>

469

470 Relationships between fractal constants of BSf derived from the fits of this model to the  
471 adsorption data,  $\tau_c$  and  $\alpha$ , and their physicochemical properties of ACs,  $S_{DFT}$  and surface  
472 functional groups, were looked for. Gaspard et al. (Gaspard et al. 2006) already showed that  
473 BSf parameters are indeed correlated with the fractal dimension  $D$  for the adsorption of  
474 phenol and tannic acid onto three commercial ACs, and onto two ACs derived from *Vetiveria*  
475 *zizanioides*.

476 **Fig 6** shows the effect of  $S_{DFT}$  and surface functional groups on the BSf(1, $\alpha$ ) constants  $\tau_c$   
477 and  $\alpha$  for the adsorption of MB and MO dyes. Certain correlation between  $\alpha_{MB}$ ,  $\alpha_{MO}$  and  $S_{DFT}$   
478 and amount of functional groups can be seen. The constant  $\tau_c$  is also clearly correlated with  
479  $S_{DFT}$  and with the amount of functional groups. Constant  $\alpha$  is always inferior to 1 ( $0.51 < \alpha <$   
480  $0.99$ ) for the adsorption of MB onto F300 and Cecalite® and for the adsorption of MO onto  
481 F200, F300 and Cecalite®, clearly suggesting fractal adsorption. In contrast, for the  
482 adsorption of MB onto Acticarbone® and F200, and for the adsorption of MO onto  
483 Acticarbone®, the kinetic is not clearly fractal because the constant  $\alpha$  is higher than 1  
484 (Brouers et al. 2005; Ben Hamissa et al. 2013; Brouers 2014a).

485

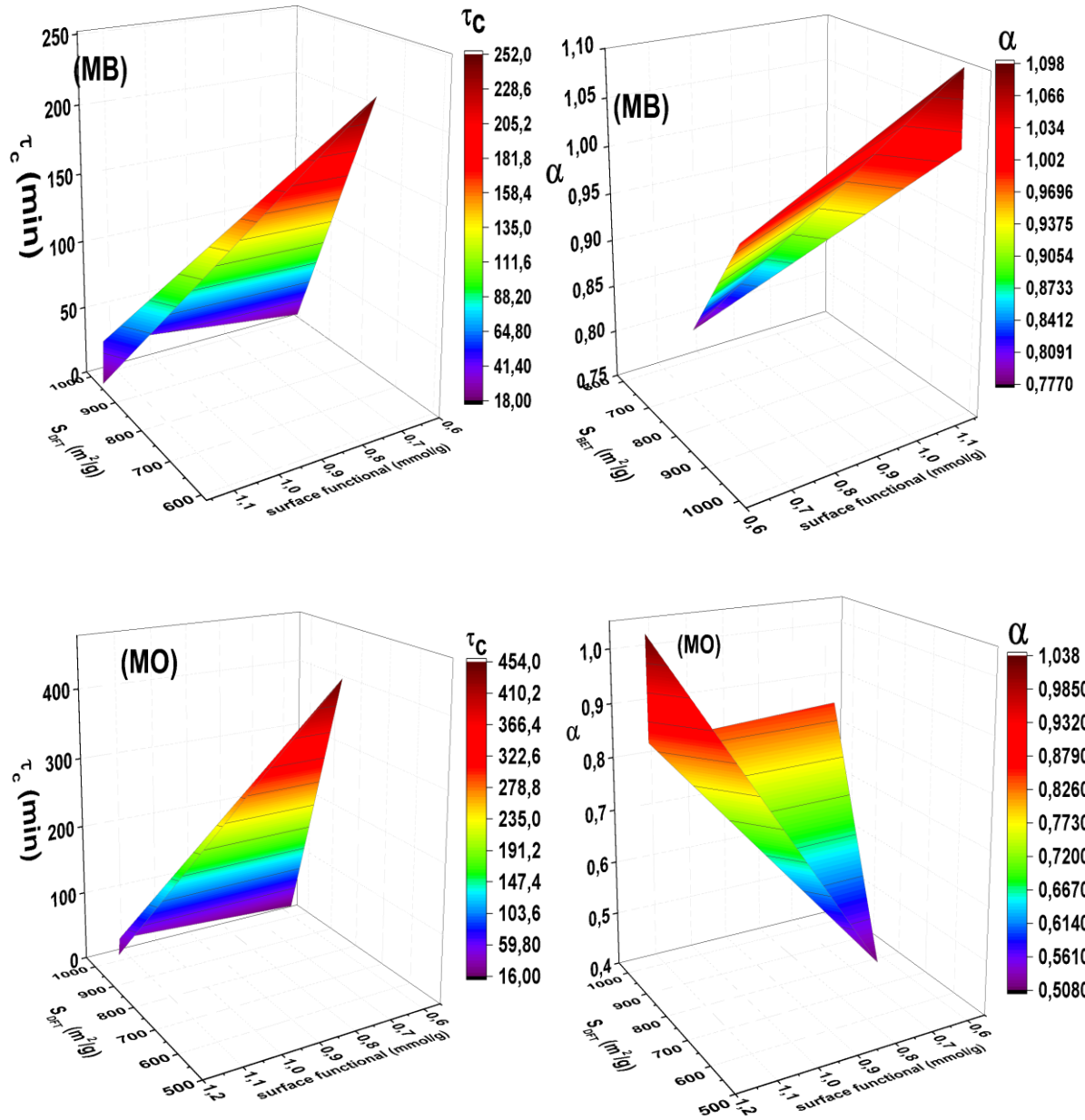


**Fig 6** Effect of  $S_{DFT}$  and amount of surface functional groups on the BSf(1, $\alpha$ ) constants  $\tau_c$  and  $\alpha$  determined by adsorption of MB at pH 8 (top) and of MO at pH 2.5 (bottom) ( $C_0 = 40$  mg.L<sup>-1</sup>, 25°C).

On one hand, the increase of  $S_{DFT}$  makes the initial speed of the adsorption increase, and consequently the characteristic time of adsorption  $\tau_c$  of MO and MB decreases. Therefore, the time of half-reaction also decreases. On the other hand, the increase of the amount of surface functional groups increases the characteristic time  $\tau_c$  towards an extremum before decreasing.

Despite the increase of the amount of surface functional groups from 0.60 to 0.79 mmol.g<sup>-1</sup> from F300 to Cecalite®, F300 being more porous than Cecalite®, the characteristic time increased from 22 to 251 min for MB adsorption, and from 17 to 452 min for MO adsorption. This shows that the effect of porosity is much more important than that of surface chemistry in agreement with previous studies (Brouers, Al-Musawi 2015; Jaramillo et al. 2012), and suggests that electrostatic interactions have a poor influence for retaining MB and MO at the surface of the ACs used. In other words, the surface functional groups have a significant impact on the kinetics of adsorption, but that of the nature of the porosity is even more important (Mailler et al. 2016).

The fractal constant  $\alpha$  increases with the specific surface area,  $S_{DFT}$ , due to the difference of porosity between the materials. This suggests that the fractal character of the surface increases due to its higher geometrical heterogeneity (Brouers, Al-Musawi 2015). Moreover, this result was also confirmed by the increase of  $\alpha$  with the number of functional surface groups, leading to chemical heterogeneity (Kesraoui et al. 2016). Finally, it can be noticed that the degree of fractality,  $\alpha$ , and the characteristic time,  $\tau_c$ , are inversely proportional to the number of functional groups.

### 3.2.3 Adsorption isotherms

A stochastic analysis of physicochemical reactions in complex systems (Stanislavsky, Weron 2013) showed that the exponent  $c$  is related to clustering or agglomeration at the surface of the adsorbent (i.e., the constant  $c$  gives an idea of the degree of heterogeneity of the adsorbent since its value is inversely proportional to the surface heterogeneity). **Table 6** shows the effect of changing the constant  $c$  in the GBS model on the quality of the fits, seen through the resultant changes of determination coefficient,  $R^2$ . The fits were performed with  $c = 0, 0.5$  and  $1$  (i.e., correspond to BS, BG and HS isotherm models, respectively), and the best ones were obtained with the BS model ( $c = 0$ ) for the adsorption of

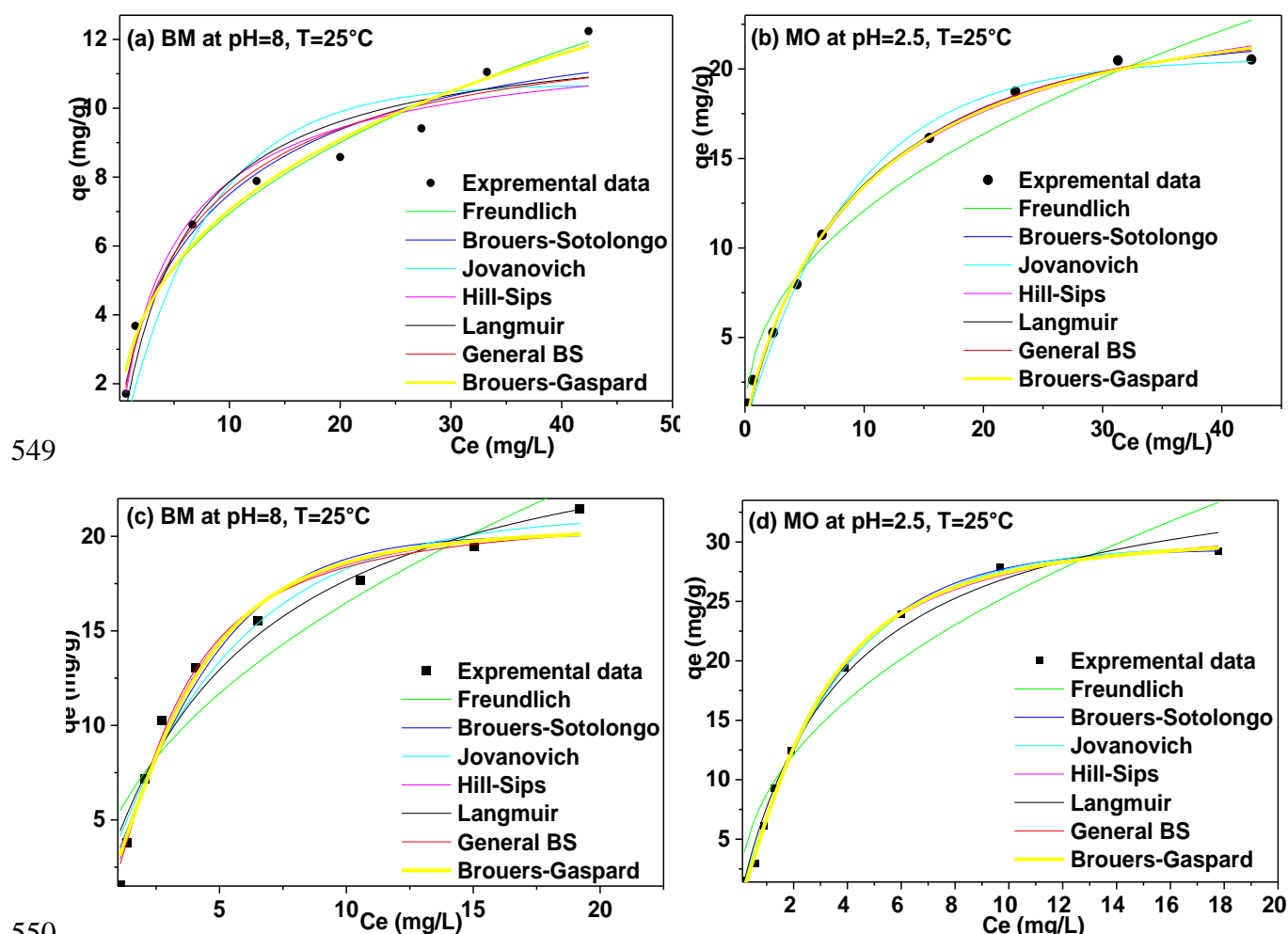
MB on all ACs except F300, best described by HS model ( $c = 1$ ). Similar results were obtained when  $Pb^{2+}$  was biosorbed onto algal biomass (Brouers, Al-Musawi 2015). The isotherms of MO adsorption onto F200 and Acticarbone® were best described by BG isotherm ( $c = 0.5$ ). MB and MO adsorption isotherms onto F300 were very well described by the HS model, indicating a poorly heterogeneous surface. In contrast, MB and MO isotherms adsorption onto Cecalite® were best fitted by the BS model, indicating the high heterogeneity of the surface. Generally, MB and MO adsorption isotherms onto all samples were adequately described by HS, BG and BS models, indicating the presence of active sites with heterogeneous sorption interactions (Brouers, Al-Musawi 2015).

**Table 6:** Effect of constant  $c$  of GBS isotherm model obtained by non-linear fit of adsorption data of MB at pH 8 and MO at pH 2.5 onto all ACs at 25°C.

GBS		$R^2$			
		F200	F300	Acticarbone®	Cecalite®
MB	$c = 0$	<u>0.998</u>	0.961	<u>0.983</u>	<u>0.970</u>
	$c = 0.5$	0.997	0.976	0.971	0.969
	$c = 1$	0.996	<u>0.983</u>	0.979	0.970
MO	$c = 0$	0.998	0.989	0.997	<u>0.997</u>
	$c = 0.5$	<u>0.998</u>	0.993	<u>0.998</u>	0.995
	$c = 1$	0.998	<u>0.995</u>	0.997	0.994

In order to compare the stochastic isotherm models to more classical models, and to avoid deciding between BS and HS models whose fits are equally good, the BG model was used (Brouers, Al-Musawi 2015) (i.e., with the constant  $c$  fixed at 0.5). **Fig 7** shows the fit of the adsorption data of MB at pH 8 and MO at pH 2.5 on Cecalite® and Acticarbone® by the models listed in the experimental section (i.e., Freundlich, Langmuir, Jovanovich, BS, HS, and BG). The corresponding models parameters and the  $R^2$  values are listed in **Table 7** and in **Table SI 7**. Based on  $R^2$ , Freundlich, Jovanovich and Langmuir models (**Table SI 7**) were not

540 appropriate for fitting MB and MO adsorption isotherms. HS and BG models seemed to be  
 541 more adequate, but the BS model gave the best fits for all pH and temperatures tested (see  
 542 **Table 7**). Brouers and Al-Musawi (Brouers,Al-Musawi 2015) explained that this finding is  
 543 related to the presence of active sites on a physically and chemically heterogeneous surface.  
 544 Chemical heterogeneity is the result of different functional groups such as carbonyls,  
 545 carboxyls, phenols, lactones, amines, aldehydes, as well as delocalised electrons determining  
 546 the more or less acidic / basic nature of ACs, as seen from the potentiometric titration  
 547 technique (Jagiello 1994). Geometrical heterogeneity is due to pores of different sizes and  
 548 morphologies (Jagiello,Olivier 2013).



551 **Fig 7** Non-linear fits of isotherm data at 25°C by several isotherm models for the adsorption  
 552 of: (a, c) MB at pH 8, and (b, d) MO at pH 2.5 on (a, b) Cecalite® and (c, d) Acticarbone®.

554 A correlation was looked for between the constants  $a$  and  $b$ , derived from a stochastic  
555 model of GBS isotherm adsorption in the case  $c = 0.5$  (i.e., BG model), and  $S_{DFT}$  and amount  
556 of surface functional groups. Constants  $a$  and  $b$  were calculated by fitting the isotherm data of  
557 MB and MO adsorption on all ACs. **Fig 8** shows the effect of  $S_{DFT}$  and surface functional  
558 groups on the BG constants  $a$  and  $b$  for the adsorption of MB and MO dyes. Correlations were  
559 indeed observed: the constant  $a$  initially decreased with the amount of functional groups then  
560 increased, clearly proving that the reaction of adsorption was initially fast. It can be concluded  
561 that there is a close relationship between the exponent  $a$  and the fractal character of the  
562 surface due to its heterogeneity (Ben Hamissa et al. 2007). When the surface heterogeneity  
563 decreased, the exponent constant  $a$  increased.

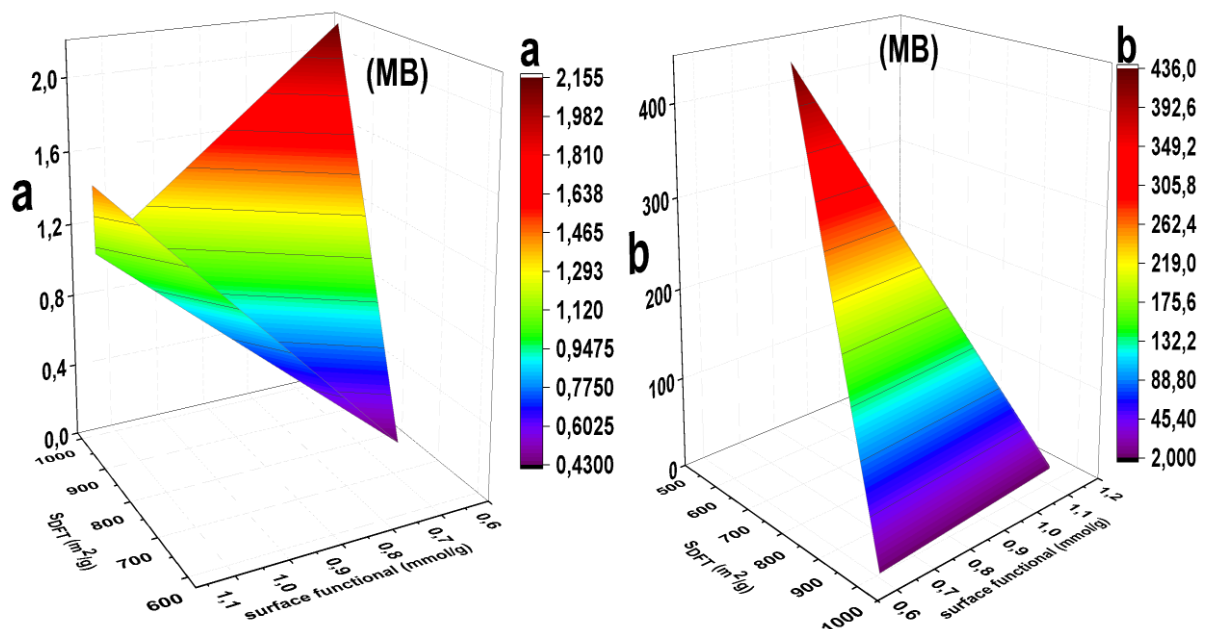
564

565 **Table 7:** Isotherm parameters of Brouers-Sotolongo, Hill-Sips and Brouers-Gaspard models  
566 fitted to the adsorption data of MB and MO at pH 8 and 2.5, respectively, and at 25°C.

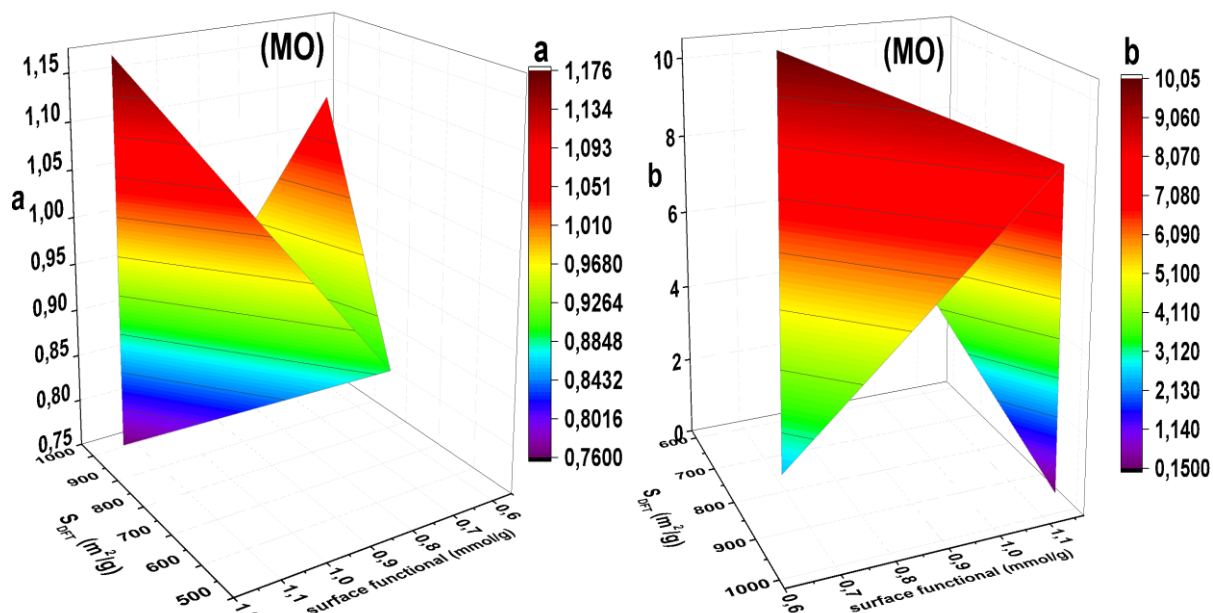
Dyes	MB				MO			
Samples	F200	F300	Acticarbhone	Cecalite	F200	F300	Acticarbhone	Cecalite
Brouers-Sotolongo								
$q_{e\ max}$	29.42	22.82	20.07	12.31	36.79	29.23	29.37	21.97
$a$	0.99	1.80	1.20	0.61	0.73	0.95	1.05	0.82
$b$	2.39	2.66	4.28	11.08	7.89	2.96	3.56	10.70
$Ce_{1/2}$	0.71	1.36	1.57	1.55	1.51	0.84	1.13	2.49
$\chi^2$	0.18	2.43	1.93	0.55	0.26	1.20	0.41	0.20
$R^2$	<u>0.998</u>	0.973	0.971	0.963	0.998	0.992	0.997	<u>0.998</u>
Hill-Sips								
$q_{e\ max}$	35.04	23.96	21.11	12.39	48.86	32.35	31.99	26.78
$a$	1.14	2.49	1.69	0.87	0.79	1.20	1.34	0.93
$b$	2.15	2.19	3.16	5.29	8.95	2.24	2.69	9.96
$Ce_{1/2}$	2.15	2.19	3.16	5.29	8.9	2.24	2.69	9.96
$\chi^2$	0.39	1.13	1.11	0.80	0.21	0.61	0.40	0.36
$R^2$	0.997	<u>0.987</u>	<u>0.983</u>	0.946	<u>0.999</u>	<u>0.996</u>	0.997	0.995
Brouers-Gaspard								
$q_{e\ max}$	32.09	23.37	20.54	41.48	42.82	30.67	30.80	24.24
$a$	1.08	2.15	1.46	0.43	0.76	1.09	1.17	0.89
$b$	2.22	2.37	3.56	434.33	8.36	2.50	3.03	10.03

$Ce_{1/2}$	1.86	2.17	3.13	280.36	6.53	2.10	2.58	8.12
$\chi^2$	0.29	1.58	1.40	0.40	0.23	0.80	0.20	0.30
$R^2$	0.997	0.976	0.971	0.969	<u>0.998</u>	0.993	<u>0.998</u>	0.995

567



568



569

570 **Fig 8** Effect of  $S_{DFT}$  and amount of surface functional groups on the GBS ( $c = 0.5$ ) constants  $a$   
571 and  $b$  determined from adsorption at 25°C of MB at pH 8 and of MO at pH 2.5.

572

573 Higher porosity of ACs increased the adsorption capacity and made the reaction faster, as  
574 observed by the increase of the constant  $a$ . Such increase is the result of geometrical

heterogeneity, which is due to differences of pores sizes and shapes, and to cracks and pits (Ncibi et al. 2008; Francois, Francisco 2016; Altenor et al. 2012). The constant  $a$  of BG mentioned in **Table 7** and the rate constants of initial kinetics of adsorption,  $h_1$  and  $h_2$  (**Table 5**), increase with the porosity of ACs (

**Table 2:** Textural characteristics of the four activated carbons obtained by adsorption-desorption of N<sub>2</sub> at -196°C and of CO<sub>2</sub> at 0°C, applying BET, DR and 2D-NLDFT methods.

Materials	$A_{BET}$ (m <sup>2</sup> .g <sup>-1</sup> )	$S_{DFT}$ (m <sup>2</sup> .g <sup>-1</sup> )	$V_{DR, N_2}$ (cm <sup>3</sup> .g <sup>-1</sup> )	$V_{DR, CO_2}$ (cm <sup>3</sup> .g <sup>-1</sup> )	$V_{0.97}$ (cm <sup>3</sup> .g <sup>-1</sup> )	$V_{\mu, NLDFT}$ (cm <sup>3</sup> .g <sup>-1</sup> )	$V_{mes}$ (cm <sup>3</sup> .g <sup>-1</sup> )	$V_{mes}$ (%)
F200	795	971	0.28	0.24	0.39	0.30	0.09	22
F300	884	1003	0.35	0.28	0.43	0.34	0.09	21
Acticarbone®	1014	967	0.35	0.18	0.56	0.38	0.16	29
Cecalite®	582	830	0.22	0.23	0.24	0.24	0.01	3

**Fig 2d** shows the PSDs obtained by mercury porosimetry. The highest porosity, i.e., the volume fraction of macropores and of mesopores available to mercury, corresponds to Acticarbone®, around 54.3 %. The porosity measurable with this technique for the other ACs was 39.7%, 35.3% and 38.0% for F200, F300 and Cecalite®, respectively. The mercury intrusion-extrusion curves are given in **Fig SI 4** of the supplementary information, evidencing the entrapment of mercury when the pressure was decreased. This finding suggests the presence of a significant amount of ink bottle-shaped pores, but also that irreversible compression may have occurred under pressure. More information is also given in **Table SI 2**, suggesting that all ACs are different either in terms of macro/mesopore size (e.g. when F200 and Cecalite® are compared) or in terms of amounts of pores of similar sizes (e.g. when F300 and Acticarbone® are compared).



). However, when  $a < 1$ , a slow initial sorption kinetics is observed and all sites don't have the same energy as assumed by Langmuir (Langmuir 1918), whereas when  $a > 1$ , a fast initial sorption kinetics occurs and there is probably more than one molecule sorbed by active site. It can be concluded that the exponent  $a$  expresses the fractal properties of a heterogeneous system and of its related adsorption mechanisms (Brouers 2014a; Kesraoui et al. 2016; Brouers, Al-Musawi 2015; Francois, Francisco 2016).

Regarding the constant  $b$ , **Fig 8** shows that the increase of the porosity from Cecalite® to Acticarbone® decreased the constant  $b$  from 10.05 to 0.15 mg/L for MO, and from 436.00 to 2.00 mg.L<sup>-1</sup> for MB. However, there is no clear effect of the amount of functional surface groups on the constant  $b$ , making difficult to establish whether porosity has a predominant role over surface functions in that case (Jaramillo et al. 2012; Brouers, Al-Musawi 2015).

#### 4. Conclusions

In the present study, four micro/mesoporous activated carbons (ACs: Acticarbone® and Cecalite® from CECA Company, and F300 and F200 from Calgon Corporation) were thoroughly characterised. From the many different techniques that were used, the main porous, structural, nanotextural and physicochemical features of those materials could be accurately determined.

Their adsorption properties with respect to methylene blue (MB) and methyl orange (MO) were investigated at different pH and temperatures. For all ACs, both MB and MO uptakes increased with temperature. However, due to the different cationic / anionic natures of those dyes, the adsorption of MB increased with pH, whereas that of MO decreased with pH.

The thermodynamics studies revealed that the adsorption process is spontaneous and endothermic, and the kinetic studies showed that, in all cases, the Brouers-Sotolongo fractal

kinetic model (BSf) was the best for describing the adsorption process. Although changing the reaction order  $n$  had a low impact on the quality of the fits, suggesting that this parameter is not very important, the best results were most of the time obtained with  $n = 1$ . The fractal time parameter  $\alpha$  of the BSf kinetic model increased with both surface area and amount of surface functional groups of the AC, due to the correspondingly increased geometrical and chemical heterogeneity.

The adsorption isotherm studies showed that both Brouers-Sotolongo (BS) and Hill-Sips (HS) models fitted the experimental data quite well. For comparing those stochastic models with more classical ones, and as it was difficult to decide between BS and HS isotherms, we fixed the parameter  $c = 0.5$ , thus corresponding to the Brouers-Gaspard (BG) equation. It was seen that the constant  $a$  of the model decreased with the amount of surface functional groups, but increased with the surface area. Now,  $a < 1$  suggests a slow initial sorption and that all the sites do not have the same energy, whereas  $a > 1$  corresponds to a fast initial sorption and to more than one molecule sorbed by active site. The behaviour experimentally observed for  $a$  thus indicates that the latter is a measure of the scaling (fractal) properties of the AC surface. The parameter  $c$  of the same model is related to the agglomeration and clustering of AC particles, or to the fractal distribution of mesopores. The constants of the BG isotherm could also be correlated with physicochemical characteristic of the ACs.

To sum up, the stochastic and fractal models of Brouers-Sotolongo, which are non-empirical complex models established from a probabilistic calculation, are the most adequate to describe the adsorption of dyes on ACs, and provide a meaningful physicochemical explanation of the different adjustable parameters. However, more investigations based on microscopy observations are needed to confirm the relationships between the constant  $c$  and agglomeration of AC particles or fractal distribution of pores. Another point to be studied is the determination of the adsorption energy distributions. These objectives will be fulfilled in

642 the near future, as well as the search for possible correlations between pH and temperature  
643 and the stochastic parameters.

#### 644 **Supplementary information**

645 SI includes results and discussion on ACs characterisation by elemental analysis,  
646 thermogravimetric analysis in air, Raman spectroscopy, XRD, potentiometric titration and  
647 intrusion-extrusion of mercury.

#### 648 **Acknowledgements**

649 The Tunisian group gratefully acknowledges the financial support of the EU-METALIC  
650 Erasmus Mundus project, and of the Tunisian Ministry of Higher Education and Scientific  
651 Research. The French group gratefully acknowledges the financial support of the CPER 2007-  
652 2013 “Structuring the Competitiveness Fibre Cluster”, through local (Conseil Général des  
653 Vosges), regional (Région Lorraine), national (DRRT and FNADT) and European (FEDER)  
654 funds.

655

## References

- Acosta, R., Fierro, V., Martinez de Yuso, A., Nabarlantz, D., Celzard, A.: Tetracycline adsorption onto activated carbons produced by KOH activation of tyre pyrolysis char. *Chemosphere* **149**, 168-176 (2016).  
doi:<https://doi.org/10.1016/j.chemosphere.2016.01.093>
- Altenor, S., Ncibi, M.C., Emmanuel, E., Gaspard, S.: Textural characteristics, physiochemical properties and adsorption efficiencies of Caribbean alga *Turbinaria turbinata* and its derived carbonaceous materials for water treatment application. *Biochem Eng J* **67**, 35-44 (2012). doi:<https://doi.org/10.1016/j.bej.2012.05.008>
- Bandosz, T.J., Jagiello, J., Contescu, C., Schwarz, J.A.: Characterization of the surfaces of activated carbons in terms of their acidity constant distributions. *Carbon* **31**(7), 1193-1202 (1993). doi:[http://dx.doi.org/10.1016/0008-6223\(93\)90072-I](http://dx.doi.org/10.1016/0008-6223(93)90072-I)
- Bello, O.S., Bello, I.A., Adegoke, K.A.: Adsorption of dyes using different types of sand: A review. *S Afr J Chem* **66**, 00-00 (2013)
- Ben Hamissa, A.M., Brouers, F., Borhane, M., Seffen, M.: Adsorption of Textile Dyes Using *Agave Americana* (L.) Fibres: Equilibrium and Kinetics Modelling. *Adsor Sci Technol* **25**(5), 311-325 (2007). doi:10.1260/026361707783432533
- Ben Hamissa, A.M., Brouers, F., Ncibi, M.C., Seffen, M.: Kinetic Modeling Study on Methylene Blue Sorption onto *Agave americana* fibers: Fractal Kinetics and Regeneration Studies. *Sep Sci Technol* **48**(18), 2834-2842 (2013).  
doi:10.1080/01496395.2013.809104
- Benaddi, H., Bandosz, T.J., Jagiello, J., Schwarz, J.A., Rouzaud, J.N., Legras, D., Béguin, F.: Surface functionality and porosity of activated carbons obtained from chemical activation of wood. *Carbon* **38**(5), 669-674 (2000).  
doi:[http://dx.doi.org/10.1016/S0008-6223\(99\)00134-7](http://dx.doi.org/10.1016/S0008-6223(99)00134-7)
- Bouhamed, F., Elouear, Z., Bouzid, J., Ouddane, B.: Multi-component adsorption of copper, nickel and zinc from aqueous solutions onto activated carbon prepared from date stones. *Environ Sci Pollut Res* **23**(16), 15801-15806 (2016). doi:10.1007/s11356-015-4400-3
- Braghiroli, F.L., Fierro, V., Parmentier, J., Vidal, L., Gadonneix, P., Celzard, A.: Hydrothermal carbons produced from tannin by modification of the reaction medium: Addition of H<sup>+</sup> and Ag<sup>+</sup>. *Ind Crops Prod* **77**, 364-374 (2015).  
doi:10.1016/j.indcrop.2015.09.010

689 Brouers, F.: The fractal (BSf) kinetics equation and its approximations. *J Mod Phys* **5**(16),  
690 1594 (2014a). doi:[doi.org/10.4236/jmp.2014.516160](https://doi.org/10.4236/jmp.2014.516160)

691 Brouers, F.: Statistical foundation of empirical isotherms. *Open J Stat* **4**(09), 687-701 (2014b).  
692 doi:<http://dx.doi.org/10.4236/ojs.2014.49064>

693 Brouers, F., Al-Musawi, T.J.: On the optimal use of isotherm models for the characterization  
694 of biosorption of lead onto algae. *J Mol Liq* **212**, 46-51 (2015).  
695 doi:[10.1016/j.molliq.2015.08.054](https://doi.org/10.1016/j.molliq.2015.08.054)

696 Brouers, F., Sotolongo-Costa, O.: Generalized fractal kinetics in complex systems  
697 (application to biophysics and biotechnology). *Phys A: Stat Mech Appl* **368**(1), 165-  
698 175 (2006). doi:<http://doi.org/10.1016/j.physa.2005.12.062>

699 Brouers, F., Sotolongo-Costa, O., Weron, K.: Burr, Lévy, Tsallis. *Phys A: Stat Mech Appl*  
700 **344**(3), 409-416 (2004). doi:[doi.org/10.1016/j.physa.2004.06.008](https://doi.org/10.1016/j.physa.2004.06.008)

701 Brouers, F., Sotolongo, O., Marquez, F., Pirard, J.P.: Microporous and heterogeneous surface  
702 adsorption isotherms arising from Levy distributions. *Phys A: Stat Mech Appl* **349**(1-  
703 2), 271-282 (2005). doi:<http://doi.org/10.1016/j.physa.2004.10.032>

704 Centeno, T.A., Stoeckli, F.: The assessment of surface areas in porous carbons by two model-  
705 independent techniques, the DR equation and DFT. *Carbon* **9**(48), 2478-2486 (2010)

706 Choi, Y.-K., Cho, M.-H., Kim, J.-S.: Air gasification of dried sewage sludge in a two-stage  
707 gasifier. Part 4: Application of additives including Ni-impregnated activated carbon  
708 for the production of a tar-free and H<sub>2</sub>-rich producer gas with a low NH<sub>3</sub> content.  
709 *Internat J Hydr Energ* **41**(3), 1460-1467 (2016).  
710 doi:<http://doi.org/10.1016/j.ijhydene.2015.11.125>

711 Dubinin, M.M.: In homogeneous microporous structures of carbonaceous adsorbents. *Carbon*  
712 **19**, 321-324 (1981)

713 Enaïme, G., Ennaciri, K., Ounas, A., Baçaoui, A., Seffen, M., Selmi, T., Yaacoubi, A.:  
714 Preparation and characterization of activated carbons from olive wastes by physical  
715 and chemical activation: Application to Indigo carmine adsorption. *J Mater Environ*  
716 *Sci* **8**(11), 4125-4137 (2017)

717 Francois, B., Francisco, M.-M.: Dubinin isotherms versus the Brouers–Sotolongo family  
718 isotherms: A case study. *Adsor Sci Technol* **34**(9-10), 552-564 (2016).  
719 doi:[doi.org/10.1177/0263617416670909](https://doi.org/10.1177/0263617416670909)

720 Freundlich, H.: Over the adsorption in solution. *J Phys Chem* **57**, 385-471 (1906)

Gaspard, S., Altenor, S., Passe-Coutrin, N., Ouensanga, A., Brouers, F.: Parameters from a new kinetic equation to evaluate activated carbons efficiency for water treatment. *Water. Res.* **40**(18), 3467-3477 (2006). doi:10.1016/j.watres.2006.07.018

Ho, Y.S., McKay, G.: Sorption of dye from aqueous solution by peat. *Chem Eng J* **70**(2), 115-124 (1998). doi:[http://doi.org/10.1016/S0923-0467\(98\)00076-1](http://doi.org/10.1016/S0923-0467(98)00076-1)

Ho, Y.S., McKay, G.: Pseudo-second order model for sorption processes. *Process Biochem* **34**(5), 451-465 (1999). doi:[http://doi.org/10.1016/S0032-9592\(98\)00112-5](http://doi.org/10.1016/S0032-9592(98)00112-5)

Húmpola, P., Odetti, H., Moreno-Piraján, J.C., Giraldo, L.: Activated carbons obtained from agro-industrial waste: textural analysis and adsorption environmental pollutants. *Adsorption* **22**(1), 23-31 (2016). doi:10.1007/s10450-015-9728-y

IUPAC: International Union of Pure and Applied Chemistry; Korean Chemical Society. In: 45th IUPAC World Chemistry Congress, Busan, Korea, 9-14 August 2015 2015. Elseviers

Jagiello, J.: Stable Numerical Solution of the Adsorption Integral Equation Using Splines. *Langmuir* **10**(8), 2778-2785 (1994). doi:10.1021/la00020a045

Jagiello, J., Ania, C., Parra, J.B., Cook, C.: Dual gas analysis of microporous carbons using 2D-NLDFT heterogeneous surface model and combined adsorption data of N<sub>2</sub> and CO<sub>2</sub>. *Carbon* **91**, 330-337 (2015). doi:10.1016/j.carbon.2015.05.004

Jagiello, J., Bandosz, T.J., Putyera, K., Schwarz, J.A.: Determination of proton affinity distributions for chemical systems in aqueous environments using a stable numerical solution of the adsorption integral equation *J Colloid Interface Sci* **172**, 341-346 (1995)

Jagiello, J., Bandosz, T.J., Schwarz, J.A.: Carbon surface characterization in terms of its acidity constant distribution. *Letters to the editor / Carbon*, 1026-1028 (2000)

Jagiello, J., Olivier, J.P.: 2D-NLDFT adsorption models for carbon slit-shaped pores with surface energetical heterogeneity and geometrical corrugation. *Carbon* **55**, 70-80 (2013). doi:10.1016/j.carbon.2012.12.011

Jaramillo, M.M., Mendoza, A., Vaquero, S., Anderson, M., Palma, J., Marcilla, R.: Role of textural properties and surface functionalities of selected carbons on the electrochemical behaviour of ionic liquid based-supercapacitors. *RSC Adv* **2**(22), 8439-8446 (2012). doi:10.1039/C2RA21035E

Jovanović, D.S.: Physical adsorption of gases. *Kolloid-Zeitschrift und Zeitschrift für Polymere* **235**(1), 1203-1213 (1969). doi:10.1007/bf01542530

754 Kesraoui, A., Selmi, T., Seffen, M., Brouers, F.: Influence of alternating current on the  
 755 adsorption of indigo carmine. *Environ Sci Pollut Res* **24**(11), 1-11 (2016).  
 756 doi:10.1007/s11356-016-7201-4  
 757 Kopelman, R.: Fractal Reaction Kinetics. *Science* **241**, 1620-1626 (1988).  
 758 doi:doi.org/10.1126/science.241.4873.1620  
 759 Lagergren, S.: Zur Theorie der Sogenannten Adsorption Gelöster Stoffe, *Kungliga Svenska*  
 760 *Vetenskapsakade- miens. Handlingar* **24**(4), 1-39 (1898)  
 761 Langmuir, I.: The adsorption of gases on plane surfaces of glass, mica, and platinum. *J*  
 762 *American Chem Society* **40**, 1361 (1918)  
 763 Mailler, R., Gasperi, J., Coquet, Y., Buleté, A., Vulliet, E., Deshayes, S., Zedek, S., Mirande-  
 764 Bret, C., Eudes, V., Bressy, A.: Removal of a wide range of emerging pollutants from  
 765 wastewater treatment plant discharges by micro-grain activated carbon in fluidized  
 766 bed as tertiary treatment at large pilot scale. *Sci Tot Environ* **542**, 983-996 (2016).  
 767 doi:org/10.1016/j.scitotenv.2015.10.153  
 768 Meilanov, R.P., D.A Sveshnikova, Shabanov, O.M.: Fractal nature of sorption kinetics. *J Phys*  
 769 *Chem A* **106**(48), 11771–11774 (2002). doi:10.1021/jp0216575  
 770 Miao, M.-S., Liu, Q., Shu, L., Wang, Z., Liu, Y.-Z., Kong, Q.: Removal of cephalexin from  
 771 effluent by activated carbon prepared from alligator weed: Kinetics, isotherms, and  
 772 thermodynamic analyses. *Process Saf Environ Prot* **104, Part B**, 481-489 (2016).  
 773 doi:<http://doi.org/10.1016/j.psep.2016.03.017>  
 774 Ncibi, M., Altenor, S., Seffen, M., Brouers, F., Gaspard, S.: Modelling single compound  
 775 adsorption onto porous and non-porous sorbents using a deformed Weibull  
 776 exponential isotherm. *Chem Eng J* **145**(2), 196-202 (2008)  
 777 Neimark, A.: A new approach to the determination of the surface fractal dimension of porous  
 778 solids. *Phys A: Stat Mech Appl* **191**(1), 258-262 (1992).  
 779 doi:[http://dx.doi.org/10.1016/0378-4371\(92\)90536-Y](http://dx.doi.org/10.1016/0378-4371(92)90536-Y)  
 780 Pereira, L.M.: Fractal Pharmacokinetics. *Comput Math Methods in Med* **11**(2), 161-184  
 781 (2010). doi:10.1080/17486700903029280  
 782 Rodríguez, A., García, J., Ovejero, G., Mestanza, M.: Adsorption of anionic and cationic dyes  
 783 on activated carbon from aqueous solutions: Equilibrium and kinetics. *J Hazard Mater*  
 784 **172**(2–3), 1311-1320 (2009). doi:<http://doi.org/10.1016/j.jhazmat.2009.07.138>  
 785 Sandro, A., Betty Carene, Evens Emmanuel, Jacques Lambert, Jean-Jacques Ehrhardt,  
 786 Gaspard, S.: Adsorption studies of methylene blue and phenol onto vetiver roots

activated carbon prepared by chemical activation. *J Hazard Mater* **165**, 1029–1039 (2009). doi:[10.1016/j.jhazmat.2008.10.133](https://doi.org/10.1016/j.jhazmat.2008.10.133)

Seredych, M., Biggs, M.J., Bandosz, T.J.: Oxygen reduction on chemically heterogeneous iron-containing nanoporous carbon: The effects of specific surface functionalities. *Microporous Mesoporous Mater* **221**, 137-149 (2016). doi:[http://doi.org/10.1016/j.micromeso.2015.09.032](https://doi.org/10.1016/j.micromeso.2015.09.032)

Sethia, G., Sayari, A.: Activated carbon with optimum pore size distribution for hydrogen storage. *Carbon* **99**, 289-294 (2016). doi:[http://doi.org/10.1016/j.carbon.2015.12.032](https://doi.org/10.1016/j.carbon.2015.12.032)

Sips, R.: The Structure of a Catalyst Surface. *J Chem Phys* **16**(5), 490-495 (1948). doi:[org/10.1063/1.1746922](https://doi.org/10.1063/1.1746922)

Sokolowska, Z., M. Hajnos, C. Hoffmann, M.S. Manfred, Sokolowski, S.: Comparison of fractal dimensions of soils estimated from adsorption isotherms, mercury intrusion, and particle size distribution. *J Plant Nutr Soil Sci* **164**(5), 591–599 (2001). doi:[10.1002/1522-2624\(200110\)164:5<591::AID-LPLN591>3.0.CO;2-Y](https://doi.org/10.1002/1522-2624(200110)164:5<591::AID-LPLN591>3.0.CO;2-Y)

Stanislavsky, A., Weron, K.: Is there a motivation for a universal behaviour in molecular populations undergoing chemical reactions? *Phys Chem Chem Phys* **15**(37), 15595-15601 (2013). doi:[10.1039/C3CP52272E](https://doi.org/10.1039/C3CP52272E)

Stoeckli, F.: in Porosity in carbon. Characterization and applications. J. W Patrick, London (1995)

Tian, S., Mo, H., Zhang, R., Ning, P., Zhou, T.: Enhanced removal of hydrogen sulfide from a gas stream by 3-aminopropyltriethoxysilane-surface-functionalized activated carbon. *Adsorption* **15**(5), 477 (2009). doi:[10.1007/s10450-009-9198-1](https://doi.org/10.1007/s10450-009-9198-1)

Washburn, E.W.: The dynamics of capillary flow. *Phys Rev* **17**(3), 273-283 (1921). doi:[10.1103/PhysRev.17.273](https://doi.org/10.1103/PhysRev.17.273)

Zhang, Z., Pfefferle, L., Haller, G.L.: Characterization of functional groups on oxidized multi-wall carbon nanotubes by potentiometric titration. *Catal Today* **249**, 23-29 (2015). doi:[http://doi.org/10.1016/j.cattod.2014.12.013](https://doi.org/10.1016/j.cattod.2014.12.013)



816 **Figure captions**

817 Fig 1 SEM pictures of activated carbons used here: (a) F200, (b) F300, (c) Acticarbone®, and  
818 (d) Cecalite®

819 Fig 2 Adsorption-desorption isotherms of: (a) N<sub>2</sub> at -196°C, (b) CO<sub>2</sub> at 0°C, and (c) PSDs  
820 obtained from N<sub>2</sub> and CO<sub>2</sub> adsorption data; (d) PSDs obtained by mercury intrusion

821 Fig 3 Density of functional groups of all studied ACs

822 Fig 4 Effect of: (a, b) pH at 25°C and (c, d) temperature, on the adsorbed amount at  
823 equilibrium of: (a, c) MB at pH 8, and (b, d) MO at pH 2.5, onto all ACs ( $C_0 = 40 \text{ mg.L}^{-1}$ )  
824 <sup>1</sup>)

825 Fig 5 BSf (1,α) kinetics model applied to the adsorption of: (a) MB at pH 8 and (b) MO at pH  
826 2.5, onto Acticarbone® for different initial concentrations at 25°C

827 Fig 6 Effect of  $S_{DFT}$  and amount of surface functional groups on the BSf(1,α) constants  $\tau_c$  and  
828  $\alpha$  determined by adsorption of MB at pH 8 (top) and of MO at pH 2.5 (bottom) ( $C_0 = 40$   
829  $\text{mg.L}^{-1}$ , 25°C)

830 Fig 7 Non-linear fits of isotherm data at 25°C by several isotherm models for the adsorption  
831 of: (a, c) MB at pH 8, and (b, d) MO at pH 2.5 on (a, b) Cecalite® and (c, d)  
832 Acticarbone®

833 Fig 8 Effect of  $S_{DFT}$  and amount of surface functional groups on the GBS ( $c = 0.5$ ) constants  $a$   
834 and  $b$  determined from adsorption at 25°C of MB at pH 8 and of MO at pH 2.5

835

836

837 **List of tables**

838 Table 1: Main characteristics of dyes used in the present work.

839 Table 2: Textural characteristics of the four activated carbons obtained by adsorption-  
840 desorption of N<sub>2</sub> at -196°C and of CO<sub>2</sub> at 0°C, applying BET, DR and 2D-NLDFT  
841 methods.

842 Table 3: Thermodynamic parameters for the adsorption of MB and MO onto all activated  
843 carbons samples at different temperatures and C<sub>0</sub> = 40 mg.L<sup>-1</sup>.

844 Table 4: Effect of reaction order n on BSf kinetics parameters obtained by non-linear fit of the  
845 adsorption of MB at pH 8 and MO at pH 2.5 on Acticarbone® at 25°C.

846 Table 5: Kinetic parameters obtained by fitting the experimental data with PFO, PSO and BSf  
847 models (C<sub>0</sub> = 40 mg.L<sup>-1</sup> of MO at pH 2.5 and of MB at pH 8, at 25°C).

848 Table 6: Effect of constant c of GBS isotherm model obtained by non-linear fit of adsorption  
849 data of MB at pH 8 and MO at pH 2.5 onto all ACs at 25°C.

850 Table 7: Isotherm parameters of Brouers-Sotolongo, Hill-Sips and Brouers-Gaspard models  
851 fitted to the adsorption data of MB and MO at pH 8 and 2.5, respectively, and at 25°C.